https://doi.org/10.5194/acp-2022-427
Preprint. Discussion started: 27 June 2022

Atmospheric Chemistry and Physics Discussions

Aerosol activation characteristics and prediction at the central European ACTRIS research station Melpitz, Germany

Yuan Wang[1,2,3*], Silvia Henning[1*], Laurent Poulain[1], Chunsong Lu[2], Frank Stratmann[1], Yuying Wang[2], Shengjie Niu[2,4], Mira L. Pöhlker[1], Hartmut Herrmann[1], and Alfred Wiedensohler[1]

1. Leibniz Institute for Tropospheric Research (TROPOS), 04318 Leipzig, Germany.
2. Collaborative Innovation Center on Forecast and Evaluation of Meteorological Disasters, Nanjing University of Information Science and Technology, 210044 Nanjing, China.
3. Collaborative Innovation Center for Western Ecological Safety, Lanzhou University, 730000 Lanzhou, China.
4. College of Safety Science and Engineering, Nanjing Tech University, 210009 Nanjing, China.

*Correspondence: Yuan Wang (wang_yuan@lzu.edu.cn) and Silvia Henning (henning@tropos.de)

Abstract: Understanding aerosol particle activation is essential for evaluating aerosol indirect effects (AIEs) on climate. Long-term measurements on aerosol particle activation help to understand the AIEs and narrow down the uncertainties of AIEs simulation; however, they are still scarce. In this study, more than 4-year aerosol comprehensive measurements were utilized at the central European research station Melpitz, Germany, to gain insight into the aerosol particle activation and provide recommendations on improving prediction. The overall characteristics of aerosol particle activation at Melpitz are first summarized. For supersaturation (*SS*) levels of 0.1%, 0.2%, 0.3%, 0.5%, and 0.7%, the mean cloud condensation nuclei (CCN) number concentration (N_{CCN}) increases with the increase of *SS* from 513 to 2477 cm^{-3}, which represents 11% to 52% of the total particle number concentration with diameter ranging from 10 to 800 nm, while the hygroscopicity factor (κ) and the critical diameter (D_c) decrease from 0.28±0.08 (mean value ± one standard deviation) to 0.20±0.09 and

https://doi.org/10.5194/acp-2022-427
Preprint. Discussion started: 27 June 2022

Atmospheric Chemistry and Physics Discussions

from 177±19 to 54±8 nm, respectively. Aerosol particle activation is highly variable across seasons, especially at low *SS* conditions. At *SS* = 0.1%, the seasonal mean N_{CCN} is 681 cm^{-3} in winter, which is almost twice higher than the summer value (347 cm^{-3}); the seasonal mean activation ratio (AR) in winter (0.18) is three times higher than the summer one. Subsequently, size dependency of both κ and the state of mixing were investigated. As the particle diameter (D_p) increases, κ increases at D_p of ~40 to 100 nm and almost stays constant at D_p of 100 to 200 nm, whereas the degree of the external mixture keeps decreasing at D_p of ~40 to 200 nm. The relationships of κ vs. D_p and mixture degree vs. D_p were both fitted well by the power-law function for each season. Finally, we recommend applying the κ - D_p power-law fit for N_{CCN} prediction, which can narrow down the median uncertainty within 10% for different *SS* conditions and seasons at Melpitz; it also could be applied to predict N_{CCN} at other rural and continental regions with a similar aerosol background. Additionally, the mean κ value over D_p of 100 to 200 nm also works well on the N_{CCN} prediction when *SS* is less than 0.2%.

1. Introduction

The specific subset of aerosol particles that serves as nuclei for the condensation of water vapor, forming activated cloud droplets at a given supersaturation (*SS*) condition, is known as cloud condensation nuclei (CCN). Aerosol particle activation affects the aerosol and cloud interactions (ACI), thereby changing the cloud microstructure (Zhao et al., 2012; Lu et al., 2013; Jia et al., 2019; Wang et al., 2019), precipitation (Khain, 2009; Wang et al., 2011; Fan et al., 2012, 2018), radiation (Twomey, 1974, 1977; Albrecht, 1989; Zhao and Garrett, 2015), and by these effects the global climate (Ramanathan et al., 2001; Wang et al., 2014; Rosenfeld et al., 2019). The latest sixth assessment report from IPCC (2021) pointed out that aerosol indirect

https://doi.org/10.5194/acp-2022-427
Preprint. Discussion started: 27 June 2022


Atmospheric Chemistry and Physics Discussions

effects (AIEs) remain the most considerable uncertainty in assessing the anthropogenic contribution to present and future climate change.

The ambient *SS* and aerosol activation ability are both important for predicting the number concentration of activated droplets. The classical Köhler theory (Köhler, 1936), combining the Raoult law with the Kelvin effect, illustrates that the aerosol particle activation depends on particle size, chemical composition and the given *SS*. Petters and Kreidenweis (2007) utilized a single hygroscopicity factor κ to describe the CCN activity at each particle diameter (D_p), which facilitates studying the activation process without considering the complex chemical compositions of aerosol particles (McFiggans et al., 2006).

Different perspectives have been presented on the influence of particle size and composition on the CCN activation. In terms of a single aerosol particle, the actual particle size plays a more important role than the chemical composition for activation because of the reciprocal relationship between κ and D_p^3 at a given *SS*. As for a population of aerosol particles, Dusek et al. (2006) concluded that particle number size distribution (PNSD) matters more than the chemical composition distribution, which has been supported by many experiments. Even sometimes, assuming a constant κ still predicted CCN number concentration (N_{CCN}) well (e.g., Sihto et al., 2011; Wang et al., 2018a). Andreae and Rosenfeld (2008) reviewed the previous studies on aerosol particle activation and recommended that for modeling purposes, the global κ values of 0.3±0.1 and 0.7±0.2 can be representative for continental and marine aerosol, respectively, which has been widely used to predict N_{CCN}. The regional variability should be underlined because the mean κ measured in urban, rural, and forest exhibits significant differences. For instance, Sihto et al. (2011) suggested an average κ of 0.18 to predict the CCN activation well in boreal forest conditions in Hyytiälä, Finland; a fixed κ of

https://doi.org/10.5194/acp-2022-427
Preprint. Discussion started: 27 June 2022


Atmospheric Chemistry and Physics Discussions

0.31 suffices to calculate the N_{CCN} in a suburban site located in the center of the North China Plain (Wang et al., 2018a); the mean κ is 0.5 in a near-coast and rural background station (CESAR Tower) in Netherlands (Schmale et al., 2018); the median κ ranges from 0.02 to 0.16 at SS = 0.1−1.0% in an urban background site in Budapest, Hungary (Salma et al., 2021). Therefore, the assumption of a constant κ = 0.3 may not be appropriate when trying to predict N_{CCN} for different continental regions.

Additionally, some experiments, especially conducted on more diverse particulate sources, have indicated chemistry does play an important role in N_{CCN} variability (e.g., Nenes et al., 2002; Petters and Kreidenweis, 2007; Rose et al., 2010). Not only the bulk chemical composition with a constant κ should be considered for N_{CCN} prediction, but the size-resolved chemical composition (Deng et al., 2011, 2013; Wu et al., 2016) and the mixing state should be applied (Su et al., 2010; Zhang et al., 2014). Information on the organic aerosol fraction improves N_{CCN} prediction considerably (Poulain et al., 2010; Zhang et al., 2016; Kuang et al., 2020). Freshly formed particles are about 1 nm in diameter (Kulmala et al., 2012); they must grow to tens of nanometers in diameter to serve as the effective CCN at a relatively high SS of ~1% (Dusek et al., 2006) and even larger than 200 nm to be efficient at SS less than 0.1% (Deng et al., 2013). Aerosol chemical composition changes during the growing and aging processes. For instance, κ increases with particle size caused by photochemical processes which enhance secondary inorganic species formation and go along with an increase in particle size (Massling et al., 2009; Zhang et al., 2017; Wang et al., 2018b). On the other hand, in sulfate dominated new particle formation (NPF) events with subsequent particle growth by condensation of organic vapors, the κ of small particles may exceed the κ of the larger ones (Wang et al., 2018a). If the κ of organic aerosol increases from 0.05 to 0.15, the global average aerosol radiative forcing would decrease by ~1 W m^{-2}, which is in

https://doi.org/10.5194/acp-2022-427
Preprint. Discussion started: 27 June 2022


Atmospheric Chemistry and Physics Discussions

the same order of magnitude as the overall climate forcing of anthropogenic aerosol during the industrialization period (Rastak et al., 2017).

To obtain the regional parameters of aerosol particle activation, extensive field campaigns have been conducted worldwide. Besides the significant difference in spatial, also the temporal variations of aerosol activation characteristics are essential for N_{CCN} prediction (Andreae and Rosenfeld, 2008). Most of the observations lasted 1–2 months or even less; they mainly focused on the effects of short-term weather processes or pollution events on aerosol particle activation, such as the effects of the summer monsoon (Jayachandran et al., 2017, 2020), wet removal (Croft et al., 2009), NPF events (Dusek et al., 2010; Wu et al., 2015), biomass burning (Rose et al., 2010), and aerosol particle aging as well as oxidation processes (Zhang et al., 2016, 2017). The long-term CCN concentration measurements (of at least one full year) are still rarely reported, resulting in insufficient knowledge concerning the seasonal and annual cycles of aerosol particle activation, which are also critical for model predictions and evaluations. Burkart et al. (2011) reported the particle activation in the urban background aerosol of Vienna, Austria, based on 11-month aerosol and CCN concentration measurements. Paramonov et al. (2015) reported a synthesis of CCN measurements within the EUCAARI (European Integrated project on Aerosol Cloud Climate and Air Quality interactions) network using the long-term data collected at 14 locations. Pöhlker et al. (2016) presented the climatology of CCN properties of a remote central Amazonian rain forest site using 1-year measurements. Che et al. (2017) provided the aerosol-activation properties in the Yangtze River Delta, China, based on ~1-year measurements. Using the long-term (of most > 1 year) aerosol and CCN concentration measurements from 12 sites, Schmale et al. (2018) presented the spatial differences in aerosol particle activation for various regional backgrounds. However,

https://doi.org/10.5194/acp-2022-427
Preprint. Discussion started: 27 June 2022


Atmospheric Chemistry and Physics Discussions

systematic studies focusing on the seasonal cycle of size-resolved particle activation and respective CCN predictions are still scarce in the central European continent. Such a study would be of great help for understanding ACI and narrowing down the regional uncertainties in climate predictions.

In this investigation, more than 4-year comprehensive measurements of aerosol physical, chemical, and activation properties collected at the ACTRIS (Aerosol, Clouds and Trace Gases Research Infrastructure, http://www.actris.eu/) site Melpitz, Germany, are utilized. The major objective is to gain insight into the aerosol particle activation and provide recommendations on methods for CCN predictions. We present therefore the long-term observations and seasonal cycles of various particle activation variables such as CCN number size distribution, N_{CCN}, activation ratio, critical diameter, size-resolved κ and mixing state degree. Furthermore, we evaluated the accuracy of N_{CCN} calculated from five different activation schemes and finally provide recommendations to use a power-law based parameterization for the dependence of κ on particles diameter for long-term N_{CCN} prediction at Melpitz and for other regions with a similar aerosol background condition.

2. Methodology

2.1 Experiment details

Atmospheric aerosol measurements were conducted at the Melpitz observatory (51.54°N, 12.93°E, 86 m above sea level), 50 km to the northeast of Leipzig, Germany. The aerosol particles observed at Melpitz can be regarded as representative for the central European rural background conditions (Birmili et al., 2009). The surroundings of the site are mostly pastures and forests without significant sources of anthropogenic emissions. More detailed descriptions of the Melpitz site can be found in for example, Poulain et al. (2020).

https://doi.org/10.5194/acp-2022-427
Preprint. Discussion started: 27 June 2022


Atmospheric Chemistry and Physics Discussions

This study focuses on the physicochemical properties and the activation ability of aerosol particles using the data collected at Melpitz from August 2012 to October 2016. Figure 1 demonstrates the experimental setup. All instruments were in the same container laboratory and utilized the same air inlet. Ambient aerosol particles were first pretreated through a PM_{10} Anderson inlet and an automatic aerosol diffusion dryer kept the relative humidity in sampling lines at a relative humidity less than 40% (Tuch et al., 2009). Subsequently, the aerosol flow was divided into the different instruments using an isokinetic splitter. Particle number size distributions (PNSD) were measured using a Dual-mobility particle size spectrometer (D-MPSS, TROPOS-type; Birmili et al., 1999; Wiedensohler et al., 2012) within the diameter ranging from 5 to 800 nm. An aerosol chemical species monitor (ACSM, Aerodyne Inc; Ng et al., 2011) was used to measure the chemical compositions of near-PM_1 non-refractory submicron aerosol particles (nitrate, sulfate, chloride, ammonium, and organics). A multi-angle absorption photometer (MAAP, model 5012, Thermo Scientific; Petzold and Schönlinner, 2004) was used to measure the particle light absorption coefficients and to estimate the equivalent black carbon (eBC) mass concentration. For simultaneous measurement of particle and CCN number size distributions, dried aerosol particles were passed through the bipolar charger to establish charge equilibrium (Wiedensohler, 1988) and then through a differential mobility analyzer (DMA) for selecting a monodisperse particle fraction; after the DMA the flow was divided into two parts, respectively passed through a condensation particle counter (CPC, model 3010, TSI) to measure the total number concentration of the selected monodisperse condensation nuclei (N_{CN}) and through a cloud condensation nuclei counter (CCNC, model 100, Droplet Measurement Technologies; Roberts and Nenes, 2005) to measure the N_{CCN}. Thus, the size dependent activated fraction (AF, N_{CCN}/N_{CN}) curve, i.e., the AF at a certain diameter (D_p) of dry

https://doi.org/10.5194/acp-2022-427
Preprint. Discussion started: 27 June 2022


Atmospheric Chemistry and Physics Discussions

particles, could be obtained. A total of five different *SS* conditions was set in the CCNC instrument (0.1%, 0.2%, 0.3%, 0.5%, and 0.7%). A complete *SS* cycle lasted ~2.5 hours.

All the instrumentation was frequently calibrated within the framework of the European Center for Aerosol Calibration (ECAC, https://www.actris-ecac.eu/). The ACSM was regularly calibrated according to the manufacturer's recommendations with 350 nm monodispersed ammonium nitrate and ammonium sulfate particles (Freney et al., 2019; Poulain et al., 2020). The D-MPSS was calibrated following the recommendations in Wiedensohler et al. (2018). Throughout the campaign, the CCNC was regularly calibrated following the procedures outlined in Rose et al. (2008). The measurement uncertainties of these instruments should be noted. The uncertainty in the MAAP is within 10% (Müller et al., 2011), and those in the D-MPSS and CCNC are both on the order of 10% (Wiedensohler et al., 2018; Rose et al., 2008). For the *SS* setting in CCNC, Gysel and Stratmann (2013) pointed out that an achievable accuracy in *SS* is 10 % (relative) at $SS > 0.2\%$, and less than 0.02 % (absolute) at the lower *SS*. For the ACSM data, the uncertainty in determining the total non-refractory mass is 9%; while for the individual chemical components, it is 15% for nitrate, 28% for sulfate, 36% for ammonium, and 19% for organic matter (Crenn et al., 2015).

Due to instrument failures and maintenance operations, missing measurements occurred during the campaign. Effective data coverage is shown in Figure 2. Overall, the CCNC, D-MPSS, and ACSM-MAAP captured 45578 AF curves, 103052 PNSDs, and 26876-hour aerosol chemical measurements, which covered 63%, 92%, and 77% of the campaign time, respectively. For 42% of the time all these instruments were measuring together.

2.2 Methods

Each AF curve (N_{CCN}/N_{CN} vs. D_p) was firstly corrected for multiply charged

https://doi.org/10.5194/acp-2022-427
Preprint. Discussion started: 27 June 2022


Atmospheric Chemistry and Physics Discussions

particles. Multiply (mostly doubly) charged particles appear in the AF curve as a plateau or shoulder at small diameters because they have the same electrical mobility diameter as singly charged smaller particles; thus, they are falsely selected in the DMA (Rose et al., 2008; Henning et al., 2014). For this was corrected by subtracting the multiply charged particle fraction as determined from the D-MPSS measurements from each value of N_{CCN}/N_{CN} in AF. The PNSD from the D-MPSS measurements (5 to 800 nm) are needed as the DMA-CCNC size range does not cover the large particle fraction, which is essential for the correction. Subsequently, we obtained the corrected AF curves.

Each corrected AF curve was fitted with a sigmoid function,

$$AF = \mathrm{a} + \mathrm{b}/\left(1 + \exp\left(-\frac{D_p - D_c}{\sigma_s}\right)\right) \quad (1)$$

where a and b are the lower and upper limits for calculating critical diameters (D_c) at the set-nominal SS, and σ_s is a measure for the width of the sigmoid function. This AF fit was multiplied with the PNSD to gain the CCN number size distribution and by integrating the total number of CCN, i.e., N_{CCN}.

The critical diameter (D_c) of dry particles, κ, and mixing state at each SS condition can be derived from the AF fit results. Affected by aerosol mixing, the AF rises gradually from 0 to the max (~1) rather than an intermittent mutation. D_c is defined as the diameter of the dry particles from which 50% of the particles are activated at the given SS.

The shape of the AF curve, i.e., the relative width of the AF, represents the degree of external mixture, which can be quantified by the ratio of $(D_{75} - D_{25})/D_c$ (Jurányi et al., 2013). D_{75} and D_{25} are the diameters at which 75% and 25% of the particles are activated at the given SS. Internal mixture implies that all particles with equal dry size have equal κ with $(D_{75} - D_{25})/D_c = 0$, whereas a distribution of different κ can be

https://doi.org/10.5194/acp-2022-427
Preprint. Discussion started: 27 June 2022


Atmospheric Chemistry and Physics Discussions

224 observed for externally mixed aerosol with higher $(D_{75} - D_{25})/D_c$ values. Jurányi et al.
225 (2013) confirmed the reliability of this approach by comparing the κ distributions
226 derived from parallel monodisperse CCN measurements and HTDMA measurements.
227 According to the derivation of κ-Köhler theory (Petters and Kreidenweis, 2007),
228 the κ can be calculated from D_c at a given SS:

$$\kappa = \frac{4A^3}{27{D_c}^3 \ln^2(1 + SS/100)} \tag{2a}$$

229 with

$$A = \frac{4\sigma_{s/a} M_w}{RT\rho_w} \tag{2b}$$

230 where $\sigma_{s/a}$ is the droplet surface tension (assumed to be that of pure water, 0.0728 Nm^{-2}),
231 M_w the molecular weight of water, R the universal gas constant, T the absolute
232 temperature, ρ_w the density of water, and A can be considered a function of T. Thus, the
233 size-resolved κ can be obtained at each SS cycle.
234 Besides deriving it from the monodisperse CCN measurements, κ can be
235 determined from the ACSM chemical composition measurements (κ_{chem}) using the
236 Zdanovskii–Stokes–Robinson (ZSR) mixing rule (Zdanovskii, 1948; Stokes and
237 Robinson, 1966) combined with κ-Köhler theory:

$$\kappa_{chem} = \sum_i \varepsilon_i \kappa_i \tag{3}$$

238 where κ_i and ε_i mean the κ and volume fraction for each component, respectively, and
239 i is the number of the component in the mixture. The ε_i was derived from its measured
240 component i mass concentration and density (ρ_i). A simple ion-pairing scheme (Gysel
241 et al., 2007) was used in this study with the κ_i and ρ_i values listed in Table 1 (Wu et al.,
242 2015). Note that a κ of 0.1 is used for particulate organics (Dusek et al., 2010; Gunthe

https://doi.org/10.5194/acp-2022-427
Preprint. Discussion started: 27 June 2022


Atmospheric Chemistry and Physics Discussions

et al., 2009, 2011); for black carbon, we use a κ of 0 (Rose et al., 2011; Schmale et al., 2018).

When κ is given, we can predict the N_{CCN} at each *SS*. Thereto, $D_c(\kappa, SS)$ is calculated from equation 2a. And, assuming an internal mixture, the predicted N_{CCN} is the integration of the PNSD from D_c, that is,

$$Predicted\ N_{CCN} = \int_{D_c}^{800} PNSD(D_p)dD_p \quad (4)$$

3. Results

3.1 Aerosol activation characteristics

Figure 3a presents the time series of the mean CCN number size distribution at each *SS* condition. As *SS* increases, CCN number size distribution broadens towards smaller particle sizes, causing an increase in N_{CCN} and activation ratio (AR, i.e., ratio of N_{CCN} to total aerosol number concentration with diameter ranging from 10 to 800 nm, N_{aero}). At Melpitz, the mean N_{CCN} is 513, 1102, 1466, 2020, and 2477 cm^{-3} at *SS* of 0.1%, 0.2%, 0.3%, 0.5%, and 0.7%, respectively. The mean AR ranged from 0.11 to 0.52 at *SS* = 0.1% to 0.7%. As shown in Table 2, the mean N_{CCN} measured at Melpitz is generally higher than that measured in more remote rural background stations. For instance, as *SS* increased from 0.1% to 1.0%, the mean N_{CCN} increased from 362 to 1795 cm^{-3} in Vavihill, Sweden (Fors et al., 2011) and 274 to 1128 cm^{-3} in Hyytiälä, Finland (Paramonov et al., 2015); in Southern Great Plains, USA, the mean N_{CCN} at *SS* = 0.4% was 1248 cm^{-3} (Liu and Li, 2014); the mean N_{CCN} increased from 118 to 1826 cm^{-3} as *SS* increased from 0.1% to 0.94% in Mahabaleshwar, India (Singla et al., 2017). However, the mean N_{CCN} measured at Melpitz is far lower than that measured in polluted regions. For example, in a rural site of Guangzhou, China, the mean N_{CCN} increased from 995 to 10731 cm^{-3} as *SS* increased from 0.068% to 0.67% (Rose et al.,

https://doi.org/10.5194/acp-2022-427
Preprint. Discussion started: 27 June 2022


Atmospheric Chemistry and Physics Discussions

2010); higher N_{CCN} was observed in Wuqing, China, with the mean N_{CCN} of 2192–12963 cm^{-3} at SS = 0.056–0.7% (Deng et al., 2011); in an urban site of Seoul, Korea, the mean N_{CCN} increased from 4145 to 6067 cm^{-3} as SS increased from 0.4% to 0.8% (Kim et al., 2014); in a polluted continental site of Mahabubnagar, India, the mean N_{CCN} at SS = 1.0% was ~5400 cm^{-3} (Varghese et al., 2016).

At Melpitz, aerosol activation characteristics are highly variable across seasons. At SS = 0.1%, CCN number size distribution is wider in spring and winter than in summer and autumn; the mean N_{CCN} at SS = 0.1% is 585, 347, 440, and 681 cm^{-3} in spring, summer, autumn, and winter, respectively. The mean N_{CCN} at SS = 0.1% in winter is almost twice as high as that found in summer. The highest mean AR at SS = 0.1% was 0.18 observed in winter, whereas the lowest mean AR (0.06) was observed in summer. In spring and autumn, the mean AR at SS = 0.1% is 0.1. As SS increases, CCN number size distribution gradually peaks in summer, especially at SS = 0.5% and 0.7%. At SS = 0.7%, the mean N_{CCN} is 2622, 2530, 2222, and 2495 cm^{-3}, and the mean AR is 0.49, 0.41, 0.51, and 0.68 in spring, summer, autumn, and winter, respectively.

The AR-SS and N_{CCN}-SS relationships in each season and all datasets are shown in Figures 3b and 3c. The two relationships are similar, and both can be fitted well by the power-law function (Twomey, 1959) and the error function (Pöhlker et al., 2018). The fit results are shown in Table 3. The error function fits the relationships better than the power-law function because of more parameters. The power parameter in the power-law function means the change rate of the controlled variable with the independent variable, that is the slope in a log-log coordinate system, so it is also called the slope parameter. In the power-law fits of the two relationships, the slope parameters are highest in summer and lowest in winter. Therefore, AR and N_{CCN} are most sensitive to SS in summer, whereas the opposite is true in winter. The coefficients in the power-law

https://doi.org/10.5194/acp-2022-427
Preprint. Discussion started: 27 June 2022


Atmospheric Chemistry and Physics Discussions

fits represent the AR and N_{CCN} at SS = 1%. The coefficient in AR-SS fit is highest in winter (0.89) and lowest in summer (0.61). However, the coefficient in N_{CCN}-SS fit is highest in summer (3951 cm^{-3}) and lowest in autumn (3136 cm^{-3}). Over the whole period, the mean values of the slope parameter and the coefficient in the N_{CCN}-SS power-law fit are 3497 cm^{-3} and 0.81, respectively, which are within the range of values for continental aerosol (slope parameter of 600–3500 cm^{-3} and coefficient of 0.4–0.9) reported in Seinfeld and Pandis (2016).

CCN number size distribution is a part of the particle number size distribution (PNSD), which approximately corresponds to the part of PNSD with $D_p > D_c$ when assuming particles to be internally mixed. The schematic diagram in Appendix A shows the relationship between the PNSD and the CCN number size distribution. Aerosol chemical composition determines the κ through equation 3, thereby changing D_c at a given SS condition through equation 2a. Thus, we present the time series of the PNSD and chemical compositions in Figure 4 to explain the variations in aerosol activation characteristics.

In summer, affected by the frequent NPF events (Ma et al., 2015; Wang et al., 2017), the Aitken-mode particles with D_p < 100 nm account for the largest portion of the PNSD, resulting in the highest N_{aero} with a mean value of 6224 cm^{-3} and the smallest geometric mean diameter ($GMD = \exp\left(\frac{\sum_i n_i \times lnD_i}{N_{aero}}\right)$) with a mean value of 50 nm among the four seasons. On the contrary, in winter, the mean GMD increases to 58 nm, which is the largest among the four seasons, and the N_{aero} decreases to the lowest with a mean value of 3686 cm^{-3} because of the rare NPF events. During the NPF events, only a part of newly formed particles grows to sizes larger than D_c (e.g., ~55 nm at SS = 0.7%), whereas most of the new particles are still unactivated at $SS \leq 0.5\%$. Therefore, CCN number size distribution gradually peaks as SS increases in summer, whereas AR keeps

https://doi.org/10.5194/acp-2022-427
Preprint. Discussion started: 27 June 2022


Atmospheric Chemistry and Physics Discussions

316 a minimum even at relatively high *SS* conditions as shown in Figure 3a. In winter, the
317 lowest N_{aero} and the largest *GMD* contribute to the highest AR at each *SS* condition.
318 Figure 4b shows the average changes of the aerosol particle chemical compositions
319 over a year and the estimated bulk κ_{chem} of submicron aerosol particles. At Melpitz, the
320 mean value of bulk κ_{chem} is 0.36 with one standard deviation of 0.09 over the whole
321 period; the seasonal mean κ_{chem} plus/minus one standard deviation are 0.38 ± 0.09,
322 0.29 ± 0.08, 0.36 ± 0.08, and 0.40 ± 0.08 in spring, summer, autumn, and winter,
323 respectively. Because the κ_{chem} depends on aerosol particle chemical composition
324 through equation 3, we examined the correlation between κ_{chem} and the mass fraction
325 of each component to explain the variations of κ_{chem}. As shown in Figures 5a and 5b, a
326 negative correlation between the κ_{chem} and the organic mass fraction (f_{org}) was observed,
327 while an opposite trend was found for the nitrate ($f_{nitrate}$). Additionally, the κ_{chem} is not
328 correlated with the sulfate mass fraction ($f_{sulfate}$) and the BC mass fraction (f_{BC}), as
329 shown in Figures 5c and 5d.
330 In summer, there is the lowest bulk κ_{chem} with 0.29 ± 0.08 corresponding to the
331 highest f_{org} (56% of total mass on average), which could be related to the strong
332 formation of the secondary organic aerosol. In winter, low temperatures favor the
333 particulate phase of nitrate (Poulain et al., 2011) with a mean $f_{nitrate}$ of 31%, which might
334 explain the highest κ_{chem} (0.40 ± 0.08). According to equation 2a, D_c increases as
335 κ decreases at a given *SS* condition. Thus, the lowest κ_{chem} results in the narrowest CCN
336 number size distribution and a decrease in N_{CCN} in summer, especially at relatively low
337 *SS* conditions (e.g., 0.1% and 0.2%) as shown in Figure 3a.
338 **3.2 Size-resolved particle hygroscopicity factor and mixing state**
339 The hygroscopicity factor and the mixing state directly influence the D_c and the

https://doi.org/10.5194/acp-2022-427
Preprint. Discussion started: 27 June 2022


Atmospheric Chemistry and Physics Discussions

shape of the AF curve, thereby changing the N_{CCN} at a given *SS* condition. These two parameters are not constant and both vary with particle size and season.

Figure 6a presents monthly averages of κ calculated from monodisperse CCN measurements (κ_{CCN}) at each *SS* condition, and their seasonal mean values are summarized in Table 4. At Melpitz, the mean κ_{CCN} plus/minus one standard deviation over all datasets are 0.28±0.08, 0.28±0.10, 0.24±0.10, 0.21±0.09, and 0.20±0.09 at *SS* = 0.1%, 0.2%, 0.3%, 0.5%, and 0.7%, respectively, where the mean κ_{CCN} were all less than the mean bulk κ_{chem} of 0.36. The seasonal variation of κ_{CCN} at each *SS* condition is similar to that of κ_{chem}. In summer, κ_{CCN} is lowest among the four seasons, with mean values of 0.23, 0.25, 0.21, 0.19, and 0.19 at *SS* = 0.1%, 0.2%, 0.3%, 0.5%, and 0.7%, respectively. The highest κ_{CCN} at each *SS* condition was observed in winter, with mean values of 0.32, 0.32, 0.28, 0.23, and 0.21 at *SS* = 0.1%, 0.2%, 0.3%, 0.5%, and 0.7%, respectively. κ_{CCN} in spring are slightly lower than that in winter, with mean values of 0.31, 0.32, 0.27, 0.22, and 0.21 at *SS* = 0.1%, 0.2%, 0.3%, 0.5%, and 0.7%, respectively. In autumn, the mean κ_{CCN} are 0.27, 0.26, 0.22, 0.19, and 0.19 at *SS* = 0.1%, 0.2%, 0.3%, 0.5%, and 0.7%, respectively, which is slightly higher than that observed in summer.

Figure 6b presents the monthly variation of D_c at each *SS* condition, which shows the opposite trend to κ_{CCN} - *SS* because of the negative correlation of D_c^3 vs. κ shown in equation 2a. The seasonal mean D_c are shown in Table 4. The mean D_c plus/minus one standard deviation over the whole period are 177±19, 112±14, 91±15, 67±9, and 54±8 nm at *SS* = 0.1%, 0.2%, 0.3%, 0.5%, and 0.7%, respectively. The largest D_c at each *SS* condition were observed in summer, with mean values of 187, 116, 94, 69, and 55 nm at *SS* = 0.1%, 0.2%, 0.3%, 0.5%, and 0.7%, respectively. Followed by autumn and spring, the smallest D_c at each *SS* condition was observed in winter, with mean

https://doi.org/10.5194/acp-2022-427
Preprint. Discussion started: 27 June 2022


Atmospheric Chemistry and Physics Discussions

values of 168, 107, 86, 64, and 53 nm at SS = 0.1%, 0.2%, 0.3%, 0.5%, and 0.7%, respectively.

The monthly average of the external-mixing degree is shown in Figure 6c. The degree of external mixture is quantified by the ratio of $(D_{75} - D_{25})/D_c$. The seasonal mean $(D_{75} - D_{25})/D_c$ are presented in Table 4. Jurányi et al. (2013) pointed out that the $(D_{75} - D_{25})/D_c$. ranged from 0.08 to 0.12 for ammonium sulfate calibration measurements at SS = 0.1−1.0%, which indicated an internal mixture within measurement accuracy. For our measurements, the mean $(D_{75} - D_{25})/D_c$ over all datasets range from 0.17 to 0.25 at SS = 0.1−0.7%. In summer, $(D_{75} - D_{25})/D_c$ is lowest ranging from 0.14 to 0.18 at SS = 0.1−0.7%, implying that aerosol particles were extremely close to being internally mixed. Followed by spring and autumn, the highest $(D_{75} - D_{25})/D_c$ was observed in winter with values ranging from 0.24 to 0.36 at SS = 0.1−0.7%. Therefore, the results tend to indicate that the aerosol particles were less internally mixed in winter among the four seasons at Melpitz. In non-urban locations, initially externally mixed aerosol particles become an internal mixture on a time scale of ~1 day (Fierce et al., 2016). In winter, the relatively stable weather patterns increase the persistence of aerosol (> 5 days) at Melpitz (Schmale et al., 2018). When tracking an aerosol cluster, the prolonged mixing time should promote the aging process, leading to an internal mixture. However, we observed a less internally mixed aerosol particle population in winter. A plausible explanation is mixing in of local pollution.

Essentially, the relationship between κ_{CCN} and SS is determined by the κ_{CCN} vs. D_p relationship. Identically, the relationship between $(D_{75} - D_{25})/D_c$ and SS depends on the $(D_{75} - D_{25})/D_c$ vs. D_p relationship. Monodisperse CCN measurements provide the size-resolved κ and $(D_{75} - D_{25})/D_c$. At a given SS condition, κ_{CCN} represents the κ of particles at $D_p = D_c$, and the same is true for $(D_{75} - D_{25})/D_c$. It should be noted that our

https://doi.org/10.5194/acp-2022-427
Preprint. Discussion started: 27 June 2022


Atmospheric Chemistry and Physics Discussions

monodisperse CCN measurements only provide the size-resolved κ and $(D_{75} - D_{25})/D_c$ within D_p of ~40−200 nm.

As shown in Figure 7a, κ_{CCN} increases with D_p at D_p of ~40 to 100 nm, whereas κ_{CCN} almost stays constant at D_p of 100 to 200 nm for all seasons. Additionally, the increase κ_{CCN} with D_p varies with season. The κ_{CCN} vs. D_p relationship is fitted by a power-law function at each season. Fit results are presented in Table 5. In summer, there is the lowest slope parameter of 0.19 in the κ_{CCN} vs. D_p power-law fit, meaning that the difference between the κ_{CCN} at different particle sizes is smallest among the four seasons. Followed by autumn with the slope parameter of 0.31, the slope parameter is highest in spring and winter of 0.36−0.37. Therefore, the κ_{CCN} is most sensitive to D_p in spring and winter.

Figure 7b presents the $(D_{75} - D_{25})/D_c$ vs. D_p relationship. As particle size increases, $(D_{75} - D_{25})/D_c$ decreases at D_p of ~40 to 200 nm for all seasons, meaning that small particles are less internally mixed. The reason is that during the aerosol aging process, not only particle size increases but κ becomes more uniform. The $(D_{75} - D_{25})/D_c$ vs. D_p relationship is also fitted well by the power-law function at each season, with fit results shown in Table 5. The highest absolute value of the slope parameter was observed in autumn of 0.42, followed by winter of 0.30 and spring of 0.26, and the lowest was 0.20 observed in summer. Thus, the difference between the degree of external mixture at different particle sizes is largest in autumn, followed by winter and spring, and is smallest in summer.

3.3 N_{CCN} prediction at Melpitz

N_{CCN} plays an important role in modeling the formation and evolution of clouds (Zhao et al., 2012; Fan et al., 2012, 2018). This section evaluates the accuracy of N_{CCN} predicted from five different schemes. Table 6 introduces the five schemes, which can

https://doi.org/10.5194/acp-2022-427
Preprint. Discussion started: 27 June 2022


Atmospheric Chemistry and Physics Discussions

be summarized into two categories of N_{CCN} prediction approach. The fit results of N_{CCN} - *SS* relationship and *AR* - *SS* relationship can predict N_{CCN} at the given *SS* conditions, which belongs to the 1st category approach, corresponding to the 1st and 2nd schemes in Table 6, respectively. Compared to CCN measurements, it is generally more common and simpler to obtain the PNSD measurements; thus, we usually predict N_{CCN} using the real-time PNSD combined with the parameterized CCN activity, which belongs to the 2nd category approach. The last three schemes in Table 6 belong to the 2nd category approach, but they vary in assuming κ. The 3rd scheme uses a fixed κ of 0.3 without temporal and size-dependent variations, as recommended for continental aerosol (Andreae and Rosenfeld., 2008). The 4th scheme uses the bulk κ_{chem} calculated from aerosol chemical composition, which is also non-size-dependent but changes over time. The 5th scheme uses the κ - D_p power-law fit results shown in Table 5, which are size-dependent without temporal variations at each season. Applying the κ - D_p power-law equation into equation 2a, D_c can be derived as function of *SS*,

$$D_c = \left(\frac{4 \times A^3}{27 \times coef \times \ln^2(1 + SS/100)} \right)^{\frac{1}{slope+3}} \quad (5)$$

where the *slope* and *coef* represent the slope parameter and the coefficient in κ - D_p power-law fit. Subsequently, the predicted N_{CCN} can be calculated through equation 4. The last three schemes all assume that aerosol particles are internally mixed at a particular D_p, as used in many previous N_{CCN} prediction studies (e.g., Deng et al., 2013; Pöhlker et al., 2016; Wang et al., 2018a).

The prediction results are shown in Figure 8. The linear equation (y = kx) is used to fit the relationship between the predicted N_{CCN} and the measured one, and its slope represents the mean ratio of the predicted N_{CCN} to the measured N_{CCN}. To make the results of the predictions comparable for all regression schemes, we also applied a linear

https://doi.org/10.5194/acp-2022-427
Preprint. Discussion started: 27 June 2022


Atmospheric Chemistry and Physics Discussions

438 regression to the 1st scheme and forced the linear regression through zero for all
439 schemes. The relative deviation (RD) equals the ratio of the absolute difference between
440 the predicted N_{CCN} and the measured one to the measured N_{CCN}, i.e., RD = (|predicted
441 N_{CCN} – measured N_{CCN}|)/measured N_{CCN}; a large RD represents a large deviation
442 between prediction and measurement. The slope and RD shown in Figure 8 are both
443 calculated from all five *SS* conditions for each season. As shown in Figure 8, the 1st and
444 2nd schemes only provide rough estimates of the N_{CCN} on account of the pretty high RD
445 ranging from 64% to 136%. Compared to the 1st category approach (the 1st and 2nd
446 schemes), the 2nd category approach (the 3rd, 4th, and 5th schemes) predicts N_{CCN} better.
447 The predicted N_{CCN} correlates well with the measured one for the 3rd, 4th, and 5th
448 schemes with $R^2 > 0.97$; but N_{CCN} is generally overestimated for the 3rd and 4th schemes
449 because the fit slopes range from 1.03 to 1.17 for different seasons. The 5th scheme
450 appears to be the best one for N_{CCN} prediction among the five schemes on account of
451 the lowest RD ranging from 11% to 17% and the fit slope of ~1 for different seasons. It
452 should be noted that the fit slope shown in Figure 8 represents the average over all five
453 *SS* conditions, which could obscure the performance at each *SS* condition. Thus, Figure
454 9 further evaluates the five schemes for the N_{CCN} prediction at each *SS* condition.

455 When using the N_{CCN} - *SS* power-law fit (the 1st scheme) to predict N_{CCN}, it causes
456 significant overestimations of N_{CCN} at *SS* = 0.1% with median values ranging from 3%
457 to 29% for different seasons and causes less than 21% underestimations in median at
458 other larger *SS* conditions. Additionally, the prediction results are much uncertain at a
459 given *SS* condition and season, especially at *SS* = 0.1%. For instance, one-quarter of the
460 predicted N_{CCN} are twice higher than the measured values at *SS* = 0.1% for all datasets.
461 Thus, this scheme can only be used to provide rough estimations of N_{CCN}.

462 When using the real-time N_{aero} combined with *AR* - *SS* power-law fit (the 2nd

https://doi.org/10.5194/acp-2022-427
Preprint. Discussion started: 27 June 2022


Atmospheric Chemistry and Physics Discussions

463 scheme) to predict N_{CCN}, the performances are slightly better than those of the 1st
464 scheme. The median overestimations of N_{CCN} are less than 17% at SS = 0.1% for all
465 seasons, while the median underestimations of N_{CCN} range from 12% to 35% at SS =
466 0.2%−0.7% for all seasons. Similarly, the prediction results remain a high uncertainty
467 at a given SS condition and season. Thus, this scheme also provides rough estimations
468 on N_{CCN}.

469 When assuming the real-time PNSD combined with a constant κ of 0.3 (the 3rd
470 scheme) to predict N_{CCN}, it causes overestimations of N_{CCN} in most cases. The median
471 of the overestimation ranges from -3% to 30% at SS = 0.1%−0.7% for different seasons.
472 As shown in Figure 7a, a constant κ of 0.3 is almost greater than the κ_{CCN} of all particles
473 with the diameter ranging from ~40 to 200 nm, except for the accumulation-mode
474 particles (D_p of 100 to 200 nm) in spring and winter. Therefore, besides the well-
475 predicted N_{CCN} at SS = 0.1% and 0.2% in spring and winter, N_{CCN} is overestimated at
476 assuming a constant κ of 0.3 as shown in Figure 9c. The largest overestimation occurs
477 at SS = 0.1% in summer (30% in median) because of the low κ_{CCN} (0.22 in average)
478 combined with the low measured N_{CCN} (347 cm^{-3} in average). Although the largest
479 median overestimation reaches to 30%, which is numerically similar to the largest
480 median overestimation of the 1st scheme (29%) and the largest median underestimation
481 of the 2nd scheme (35%), the uncertainties of the 3rd scheme are much lower than those
482 of the 1st and 2nd schemes. For example, when using 3rd scheme, one-quarter of the ratio
483 of the predicted N_{CCN} to the measured N_{CCN} are larger than 1.31 at SS = 0.1% for all
484 datasets as shown in Figure 9c, while the ratio is ~2.0 for both the results of 1st and 2nd
485 scheme as shown in Figures 9a and 9b. Thus, the 3rd scheme has better predictions on
486 N_{CCN} compared to the 1st and 2nd schemes.

487 When assuming the real-time PNSD combined with the real-time bulk κ_{chem} (the

https://doi.org/10.5194/acp-2022-427
Preprint. Discussion started: 27 June 2022


Atmospheric Chemistry and Physics Discussions

488 4th scheme) to predict N_{CCN}, it also causes clear overestimations of N_{CCN} in most cases,
489 like the prediction results calculated from the 3rd scheme. The median overestimations
490 are within 7% to 21% at SS = 0.1%−0.7% for different seasons. The reason for the
491 overestimation is that the κ_{chem} is greater than κ_{CCN} measured at all the five SS
492 conditions. For instance, the mean κ_{CCN} over all datasets ranges from 0.20 to 0.28 at SS
493 = 0.1%−0.7%, whereas the mean κ_{chem} over all datasets is 0.36. The largest
494 overestimation also occurs at SS = 0.1% in summer with 21% in median. Compared to
495 the 3rd scheme, the uncertainty of the N_{CCN} prediction at a given SS condition and season
496 is lower in the 4th scheme. Considering the median overestimations of the predicted
497 N_{CCN} at different seasons and SS conditions and the uncertainty of the predicted N_{CCN} at
498 each given season and SS condition, we conclude that the performances of the 4th
499 scheme are better than the 3rd scheme.

500 When assuming the real-time PNSD combined with the κ - D_p power-law fit (the
501 5th scheme) to predict N_{CCN}, it can predict the N_{CCN} well at each SS condition for all
502 seasons. At SS = 0.1%, it causes less than 10% overestimation in median for N_{CCN}
503 prediction for all seasons; at SS = 0.2%−0.7%, the median overestimation ranges from
504 -3% to 6% for all seasons. The uncertainty of the N_{CCN} prediction at a given SS condition
505 and season is also smallest among the five schemes, especially at relatively high SS
506 conditions (e.g., 0.5% and 0.7%). For instance, at SS = 0.7% for all datasets, when using
507 the 5th scheme, one-quarter of the ratio of the predicted N_{CCN} to the measured N_{CCN} are
508 larger than 1.10, while the ratio ranges from 1.18 to 1.38 for other four schemes.
509 Therefore, the 5th scheme provides the best N_{CCN} prediction among the five schemes.

510 Overall, the performance for N_{CCN} prediction is gradually getting better from the
511 1st to the 5th scheme shown in Table 6. The classic N_{CCN} - SS and AR - SS power-law fits
512 shown in Table 3 can only be used to provide rough estimates of the N_{CCN}. At Melpitz,

https://doi.org/10.5194/acp-2022-427
Preprint. Discussion started: 27 June 2022


Atmospheric Chemistry and Physics Discussions

using a constant κ of 0.3 or the bulk κ_{chem} both causes significant overestimations of N_{CCN} with about 30% in median, especially at SS = 0.1% in summer. The κ - D_p power-law fit at each season shown in Table 5 is recommended applying for N_{CCN} prediction at Melpitz, which can narrow down the prediction deviation (ratio of the predicted N_{CCN} to the measured N_{CCN} minus 1) within 10% in median. Additionally, as shown in Figure 10, the κ - D_p power-law fit measured at Melpitz is similar to that measured at other rural and continental regions with similar aerosol background conditions, e.g., the Vavihill station in Sweden (Fors et al., 2011) and the Xinken station in China (Eichler et al., 2008), and is also valid for some urban (Ye et al., 2013) and suburb regions (Mazoyer et al., 2019). Therefore, the κ - D_p power-law fit measured at Melpitz could be applied to predict N_{CCN} for these regions. However, it may cause considerable deviations for different aerosol background regions, e.g., the polluted suburb station in Xingtai, China (Wang et al., 2018a), the coast of Barbados (Kristensen et al., 2016), the amazon rainforest (Pöhlker et al., 2016), and the urban station in Budapest, Hungary (Salma et al., 2021), because their κ - D_p relationships are different from that measured at Melpitz.

Additionally, it should be noted that the main size dependence of κ occurs at D_p of ~40 to 100 nm as shown in Figure 7a, which would be for SS larger than 0.2%. At D_p of 100 to 200 nm corresponding to SS less than 0.2%, κ almost stays constant. The mean value of κ is close to 0.3 for spring and winter, and that's where deviations in Figure 9c are small. However, the mean value of κ overestimates the κ for SS larger than 0.2% at each season. We further compare the N_{CCN} predictions between using the seasonally mean value of κ over D_p of 100 to 200 nm and the κ - D_p power-law fit. As shown in Figure 11, at SS = 0.1 and 0.2%, the seasonally mean κ value over D_p of 100 to 200 nm

https://doi.org/10.5194/acp-2022-427
Preprint. Discussion started: 27 June 2022


Atmospheric Chemistry and Physics Discussions

and κ - D_p power-law fit both predict the N_{CCN} well at each season, while the mean κ value leads to significant overestimation of N_{CCN} within 10% on average at SS = 0.3, 0.5, and 0.7%. Therefore, to predict the N_{CCN} at a relatively low SS of less than 0.2% (e.g., in fog and shallow stratiform cloud), the mean κ value over D_p of 100 to 200 nm also works well. The mean value plus/minus one standard deviation are 0.32±0.09, 0.24±0.07, 0.26±0.09, 0.32±0.10 and 0.28±0.09 for spring, summer, autumn, winter, and all datasets, respectively.

4. Conclusions

Aerosol particle activation plays an important role in determining the number concentration of cloud droplets, thereby affecting cloud microphysics, precipitation processes, radiation, and climate. To reduce the uncertainties and gain more confidence in the simulations on AIEs, long-term measurements on aerosol activation characteristics are essential; however, still rarely reported. Based on more than 4-year comprehensive measurements conducted at the central European ACTRIS site Melpitz, Germany, this study presents a systematic seasonal analysis of aerosol activation characteristics and N_{CCN} predictions.

Over the whole period, the mean N_{CCN} and AR increased from 513 to 2477 cm^{-3} and 0.11 to 0.52 with SS increasing from 0.1% to 0.7%, respectively. Aerosol activation characteristics are highly variable across seasons. At SS = 0.1%, the seasonal mean N_{CCN} is 681 cm^{-3} in winter, which is almost twice higher than the summer value (347 cm^{-3}); the seasonal mean AR is 0.18 in winter, which is three times higher than the summer value (0.06). Aerosol particle activation depends on its physical and chemical properties. Affected by the frequent NPF events, in summer, the mean N_{aero} is highest (6224 cm^{-3}) and the mean GMD is smallest (50 nm) among the four seasons. On the contrary in winter, the mean N_{aero} is lowest (3686 cm^{-3}) and the mean GMD is largest (58 nm). In

https://doi.org/10.5194/acp-2022-427
Preprint. Discussion started: 27 June 2022


Atmospheric Chemistry and Physics Discussions

summer, the mean f_{org} (56%) is highest among the four seasons, corresponding to the lowest κ_{chem} with a mean value of 0.29; in winter, the mean $f_{nitrate}$ (36%) is highest among the four seasons, which might explain the highest mean κ_{chem} (0.40). Therefore, in winter, the highest κ_{chem}, largest *GMD*, and the lowest N_{aero} cause the highest AR at each *SS* condition among the four seasons.

Both κ and the mixing state are size-dependent, thereby varying with *SS*. The mean κ is 0.28, 0.28, 0.24, 0.21, and 0.20 at *SS* = 0.1%, 0.2%, 0.3%, 0.5%, and 0.7%, respectively. D_c depends on κ at a given *SS* condition. The mean D_c is 177, 112, 91, 67, and 54 nm at *SS* = 0.1%, 0.2%, 0.3%, 0.5%, and 0.7%, respectively. For different seasons, the seasonal mean κ varies from 0.23 to 0.32 at *SS* = 0.1%, and 0.19 to 0.21 at *SS* = 0.7%; the seasonal mean D_c varies from 168 nm to 187 nm at *SS* = 0.1%, and 53 nm to 55 nm at *SS* = 0.7%. The degree of external mixture is quantified by the $(D_{75} - D_{25})/D_c$, which ranges from 0.17 to 0.25 in average over the whole period at *SS* = 0.1−0.7%. In summer, aerosol particles were extremely close to being internally mixed with $(D_{75} - D_{25})/D_c$ ranging from 0.14 to 0.18 at *SS* = 0.1−0.7%; in winter, particles were less internally mixed among the four seasons with $(D_{75} - D_{25})/D_c$ ranging from 0.24 to 0.36 at *SS* = 0.1−0.7%. As D_p increases, κ increases at D_p of ~40 to 100 nm and almost stays constant at D_p of 100 to 200 nm), and $(D_{75} - D_{25})/D_c$ decreases for all seasons. The relationships of $(D_{75} - D_{25})/D_c$ vs. D_p and κ vs. D_p are both fitted well by the power-law function for each season.

Five activation schemes are evaluated on the N_{CCN} predictions. Compared to using the classic N_{CCN} - *SS* or *AR* - *SS* power-law fits to predict N_{CCN}, the prediction is better by using the real-time PNSD combined with the parameterized κ, including a constant κ of 0.3, the bulk κ_{chem}, and the κ - D_p power-law fit. However, assuming a constant κ

https://doi.org/10.5194/acp-2022-427
Preprint. Discussion started: 27 June 2022


Atmospheric Chemistry and Physics Discussions

of 0.3 recommended for continental aerosol (Andreae and Rosenfeld., 2008) or the bulk κ_{chem} calculated from aerosol chemical composition both cause significant overestimations of the N_{CCN} with about 30% in median, especially at SS = 0.1% in summer. Generally, the performances of the latter (the bulk κ_{chem}) are slightly better than the former (a constant κ of 0.3) on account of the lower uncertainty at each given season and SS condition. Size-resolved κ improves the N_{CCN} prediction. We recommend applying the κ - D_p power-law fit for N_{CCN} prediction, which obtains the best prediction among the five schemes. At Melpitz, using the real-time PNSD combined with the κ - D_p power-law fit could narrow down the uncertainty of N_{CCN} prediction within 10% in median for all SS conditions (0.1−0.7%) and seasons. The κ - D_p power-law fit presented in this study could apply to other rural and continental regions with similar aerosol background conditions. To our knowledge, the κ - D_p power-law fit is the first time applied to predict N_{CCN}. Additionally, the mean κ value over D_p of 100 to 200 nm also works well to predict N_{CCN} at a relatively low SS of less than 0.2%.

https://doi.org/10.5194/acp-2022-427
Preprint. Discussion started: 27 June 2022

Atmospheric Chemistry and Physics Discussions

Appendix B Notation list

A	comprehensive parameter for $\sigma_{s/a}$, M_w, R, T, and ρ_w in equation (2b)
a	lower limit for calculating critical diameters at the set-nominal supersaturations in equation (1)
ACI	aerosol and cloud interactions
ACSM	aerosol chemical species monitor
ACTRIS	Aerosol, Clouds and Trace Gases Research Infrastructure
AF	activated fraction, i.e., N_{CCN}/N_{CN}
AIEs	aerosol indirect effects
AR	activation ratio, i.e., N_{CCN}/N_{aero}
b	upper limit for calculating critical diameters at the set-nominal supersaturations in equation (1)
BC	black carbon
CN	condensation nuclei
CCN	cloud condensation nuclei
CCNC	cloud condensation nuclei counter
$coef$	coefficient in κ - D_p power-law fit
CPC	condensation particle counter
D_p	diameter of the dry particle
D_c	critical diameter of the dry particle
D_X	D at which X % of the particles are activated
$(D_{75} - D_{25})/D_c$	degree of external mixture
D-MPSS	Dual-mobility particle size spectrometer
DMA	differential mobility analyzer
eBC	equivalent black carbon
f_{BC}	mass fraction of BC in submicron aerosol
$f_{nitrate}$	mass fraction of nitrate in submicron aerosol
f_{org}	mass fraction of organics in submicron aerosol
$f_{sulfate}$	mass fraction of sulfate in submicron aerosol
GMD	geometric mean diameter of PNSD
M_w	molecular weight of water
N_{aero}	number concentration of aerosol with D_p ranging 10 to 800 nm
N_{CN}	number concentration of CN
N_{CCN}	number concentration of CCN
NPF	new particle formation
PM_{10}	particulate matter with the $D_p < 10$ μm
PNSD	particle number size distribution
R	universal gas constant
R^2	coefficient of determination
RD	relative deviation between the predicted N_{CCN} and the measured one
SS	supersaturation
T	temperature
σ_s	represent the shape of the sigmoid function

https://doi.org/10.5194/acp-2022-427
Preprint. Discussion started: 27 June 2022

Atmospheric Chemistry and Physics Discussions

$\sigma_{s/a}$	droplet surface tension
κ	hygroscopicity factor of aerosol particle
κ_i	κ *of* each component
κ_{CCN}	κ calculated from the monodisperse CCN measurements
κ_{chem}	κ calculated from the aerosol chemical measurements
ε_i	volume fraction of each component
ρ_w	density of the liquid water

Data availability.

The data used in this study are available from Silvia Henning (henning@tropos.de) upon request and https://doi.org/10.1594/PANGAEA.938215.

Author contributions.

AW, SH and LP designed the research. SH and LP collected the data at Melpitz. YW performed the data analysis and prepared the paper. All co-authors contributed to interpretation of the results as well as paper review and editing.

Competing interests.

The authors declare that they have no conflict of interest.

Acknowledgments.

This research has been supported by the H2020 research infrastructures (grant nos. ACTRIS (262254) and ACTRIS-2 (654109)), the European Cooperation in Science and Technology (grant no. COLOSSAL CA16109), the German Federal Environment Ministry (BMU) grants F&E 370343200 (German title: “Erfassung der Zahl feiner und ultrafeiner Partikel in der Außenluft”), 2008–2010, and F&E 371143232 (German title: “Trendanalysen gesundheitsgefährdender Fein- und Ultrafeinstaubfraktionen unter Nutzung der im German Ultrafine Aerosol Network (GUAN) ermittelten Immissionsdaten durch Fortführung und Interpretation der Messreihen”), 2012–2014, the Deutsche Forschungsgemeinschaft (*DFG*, German Research Foundation, HE

https://doi.org/10.5194/acp-2022-427
Preprint. Discussion started: 27 June 2022

6770/2), the Second Tibetan Plateau Scientific Expedition and Research Program (STEP), Grant No. 2019QZKK0602, the National Natural Science Foundation of China under grant numbers 42075066, 42075063, 42175099, and 42005067. The China Scholarship Council (no.202008320513) is acknowledged for supporting Yuan Wang financially. We thank Achim Grüner and René Rabe for the careful maintenance of the measurements on site.

https://doi.org/10.5194/acp-2022-427
Preprint. Discussion started: 27 June 2022

References

Albrecht, B. A.: Aerosols, cloud microphysics, and fractional cloudiness, Science, 245(4923), 1227–1230, https://doi.org/10.1126/ science.245.4923.1227, 1989.

Andreae, M. O. and Rosenfeld, D.: Aerosol-cloud-precipitation interactions. Part 1. The nature and sources of cloud-active particles, Earth-Sci. Rev., 89, 13–41, https://doi.org/10.1016/j.earscirev.2008.03.001, 2008.

Birmili, W., Stratmann, F., and Wiedensohler, A.: Design of a DMA-based size spectrometer for a large particle size range and stable operation, J. Aerosol Sci., 30, 549–553, https://doi.org/10.1016/S0021-8502(98)00047-0, 1999.

Birmili, W., Weinhold, K., Nordmann, S., Wiedensohler, A., Spindler, G., Müller, K., Herrmann, H., Gnauk, T., Pitz, M., Cyrys, J., Flentje, H., Nickel, C., Kuhlbusch, T. A. J., and Löschau, G.: Atmospheric aerosol measurements in the German Ultrafine Aerosol Network (GUAN): Part 1 – soot and particle number size distribution, Gefahrst. Reinh. Luft., 69, 137–145, 2009.

Burkart, J., Steiner, G., Reischl, G., and Hitzenberger, R.: Longterm study of cloud condensation nuclei (CCN) activation of the atmospheric aerosol in Vienna, Atmos. Environ., 45, 5751–5759, https://doi.org/10.1016/j.atmosenv.2011.07.022, 2011.

Che, H., Zhang, X., Zhang, L., Wang, Y., Shen, X., Ma, Q., Sun, J., Zhong, J.: Prediction of size-resolved number concentration of cloud condensation nuclei and long-term measurements of their activation characteristics, Sci. Rep., 7, 5819, https://doi.org/10.1038/s41598-017-05998-3, 2017.

Crenn, V., Sciare, J., Croteau, P. L., Verlhac, S., Fröhlich, R., Belis, C. A., Aas, W., Äijälä, M., Alastuey, A., Artiñano, B., Baisnée, D., Bonnaire, N., Bressi, M., Canagaratna, M., Canonaco, F., Carbone, C., Cavalli, F., Coz, E., Cubison, M. J., Esser-Gietl, J. K., Green, D. C., Gros, V., Heikkinen, L., Herrmann, H., Lunder, C., Minguillón, M. C., Močnik, G., O'Dowd, C. D., Ovadnevaite, J., Petit, J.-E., Petralia, E., Poulain, L., Priestman, M., Riffault, V., Ripoll, A., Sarda-Estève, R., Slowik, J. G., Setyan, A., Wiedensohler, A., Baltensperger, U., Prévôt, A. S. H., Jayne, J. T., and Favez, O.: ACTRIS ACSM intercomparison – Part 1: Reproducibility of concentration and fragment results from 13 individual Quadrupole Aerosol Chemical Speciation Monitors (Q-ACSM) and consistency with co-located instruments, Atmos. Meas. Tech., 8, 5063–5087, https://doi.org/10.5194/amt-8-5063-2015, 2015.

Croft, B., Lohmann, U., Martin, R. V., Stier, P., Wurzler, S., Feichter, J., Posselt, R., and Ferrachat, S.: Aerosol size-dependent below-cloud scavenging by rain and snow in the ECHAM5-HAM, Atmos. Chem. Phys., 9, 4653–4675, https://doi.org/10.5194/acp-9-4653-2009, 2009.

Deng, Z. Z., Zhao, C. S., Ma, N., Liu, P. F., Ran, L., Xu, W. Y., Chen, J., Liang, Z., Liang, S., Huang, M. Y., Ma, X. C., Zhang, Q., Quan, J. N., Yan, P., Henning, S., Mildenberger, K., Sommerhage, E., Schäfer, M., Stratmann, F., and Wiedensohler, A.: Size-resolved and bulk activation properties of aerosols in the North China Plain, Atmos. Chem. Phys., 11, 3835–3846, https://doi.org/10.5194/acp-11-3835-2011, 2011.

https://doi.org/10.5194/acp-2022-427
Preprint. Discussion started: 27 June 2022

667 Deng, Z. Z., Zhao, C. S., Ma, N., Ran, L., Zhou, G. Q., Lu, D. R., and Zhou, X. J.: An examination
668 of parameterizations for the CCN number concentration based on in situ measurements of
669 aerosol activation properties in the North China Plain, Atmos. Chem. Phys., 13, 6227–6237,
670 https://doi.org/10.5194/acp-13-6227-2013, 2013.
671 Dusek, U., Frank, G., Hildebrandt, L., Curtius, J., Schneider, J., Walter, S., Chand, D., Drewnick, F.,
672 Hings, S., Jung, D., Borrmann, S., and Andreae, M. O.: Size matters more than chemistry for
673 cloud-nucleating ability of aerosol particles. Science, 312(5778): 1375-1378, DOI:
674 10.1126/science.1125261, 2006.
675 Dusek, U., Frank, G., Curtius, J., Drewnick, F., Schneider, J., Kürten, A., Rose, D., Andreae, M. O.,
676 Borrmann, S., Pöschl, U.: Enhanced organic mass fraction and decreased hygroscopicity of
677 cloud condensation nuclei (CCN) during new particle formation events, Geophys. Res. Lett.
678 37 (3), doi: 10.1029/2009GL040930, 2010.
679 Eichler, H., Cheng, Y. F., Birmili, W., Nowak, A., Wiedensohler, A., Brüggemann, E., Gnauk, T.,
680 Herrmann, H., Althausen, D., Ansmann, A., Engelmann, R., Tesche, M., Wendisch, M., Zhang,
681 Y. H., Hu, M., Liu, S., and Zeng, L. M.: Hygroscopic properties and extinction of aerosol
682 particles at ambient relative humidity in South-Eastern China, Atmos. Environ., 42, 6321–6334,
683 https://doi.org/10.1016/j.atmosenv.2008.05.007, 2008.
684 Fan, J., Leung, L. R., Li, Z., Morrison, H., Chen, H., Zhou, Y., Qian, Y., and Wang, Y.: Aerosol
685 impacts on clouds and precipitation in eastern China: Results from bin and bulk microphysics,
686 J. Geophys. Res., 117, D00K36, https://doi.org/10.1029/2011JD016537, 2012.
687 Fan, J., Rosenfeld, D., Zhang, Y., Giangrande, S. E., Li, Z., Machado, L. A. T., Martin, S. T., Yang,
688 Y., Wang, J., Artaxo, P., Barbosa, H. M. J., Braga, R. C., Comstock, J. M., Feng, Z., Gao, W.,
689 Gomes, H. B., Mei, F., Pöhlker, C., Pöhlker, M. L., Pöschl, U., and Souza, R. A. F.: Substantial
690 convection and precipitation enhancements by ultrafine aerosol particles, Science, 359(6374),
691 411–418, DOI: 10.1126/science.aan8461, 2018.
692 Fierce, L., Riemer, N., and Bond, T. C.: Toward reduced representation of mixing state for
693 simulating aerosol effects on climate, Bull. Am. Meteorol. Soc., 98(5), 971–980,
694 https://doi.org/10.1175/BAMS-D-16-0028.1, 2016.
695 Fors, E. O., Swietlicki, E., Svenningsson, B., Kristensson, A., Frank, G. P., and Sporre, M.:
696 Hygroscopic properties of the ambient aerosol in southern Sweden – a two year study, Atmos.
697 Chem. Phys., 11, 8343–8361, https://doi.org/10.5194/acp-11-8343-2011, 2011.
698 Freney, E., Zhang, Y., Croteau, P., Amodeo, T., Williams, L., Truong, F., Petit, J.-E., Sciare, J., Sarda-
699 Esteve, R., Bonnaire, N., Arumae, T., Aurela, M., Bougiatioti, A., Mihalopoulos, N., Coz, E.,
700 Artinano, B., Crenn, V., Elste, T., Heikkinen, L., Poulain, L., Wiedensohler, A., Herrmann, H.,
701 Priestman, M., Alastuey, A., Stavroulas, I., Tobler, A., Vasilescu, J., Zanca, N., Canagaratna,
702 M., Carbone, C., Flentje, H., Green, D., Maasikmets, M., Marmureanu, L., Minguillon, M. C.,
703 Prevot, A. S. H., Gros, V., Jayne, J., and Favez, O.: The second ACTRIS inter-comparison
704 (2016) for Aerosol Chemical Speciation Monitors (ACSM): Calibration protocols and

https://doi.org/10.5194/acp-2022-427
Preprint. Discussion started: 27 June 2022

705 instrument performance evaluations, Aerosol Sci. Tech., 53, 830–842,
706 https://doi.org/10.1080/02786826.2019.1608901, 2019.
707 Gunthe, S. S., King, S. M., Rose, D., Chen, Q., Roldin, P., Farmer, D. K., Jimenez, J. L., Artaxo, P.,
708 Andreae, M. O., Martin, S. T., and Pöschl, U.: Cloud condensation nuclei in pristine tropical
709 rainforest air of Amazonia: size–esolved measurements and modeling of atmospheric aerosol
710 composition and CCN activity, Atmos. Chem. Phys., 9, 7551–7575,
711 https://doi.org/10.5194/acp-9-7551-2009, 2009.
712 Gunthe, S. S., Rose, D., Su, H., Garland, R. M., Achtert, P., Nowak, A., Wiedensohler, A., Kuwata,
713 M., Takegawa, N., Kondo, Y., Hu, M., Shao, M., Zhu, T., Andreae, M. O., and Pöschl, U.:
714 Cloud condensation nuclei (CCN) from fresh and aged air pollution in the megacity region of
715 Beijing, Atmos. Chem. Phys., 11, 11023–11039, https://doi.org/10.5194/acp-11-11023-2011,
716 2011.
717 Gysel, M., Crosier, J., Topping, D. O., Whitehead, J. D., Bower, K. N., Cubison, M. J., Williams, P.
718 I., Flynn, M. J., McFiggans, G. B., and Coe, H.: Closure study between chemical composition
719 and hygroscopic growth of aerosol particles during TORCH2, Atmos. Chem. Phys., 7, 6131–
720 6144, doi:10.5194/acp-7-6131-2007, 2007.
721 Gysel, M. and Stratmann, F.: WP3 – NA3: In-situ chemical, physical and optical properties of
722 aerosols, Deliverable D3.11: Standardized protocol for CCN measurements, Tech. rep., http://
723 https://actris-ecac.eu/ccn-nc.html, 2013.
724 Henning, S., Dieckmann, K., Ignatius, K., Schäfer, M., Zedler, P., Harris, E., Sinha, B., van
725 Pinxteren, D., Mertes, S., Birmili, W., Merkel, M., Wu, Z., Wiedensohler, A., Wex, H.,
726 Herrmann, H., and Stratmann, F.: Influence of cloud processing on CCN activation behaviour
727 in the Thuringian Forest, Germany during HCCT-2010, Atmos. Chem. Phys., 14, 7859–7868,
728 https://doi.org/10.5194/acp-14-7859-2014, 2014.
729 IPCC.: Climate Change 2021: The Physical Science Basis. Contribution of Working Group I to the
730 Sixth Assessment Report of the Intergovernmental Panel on Climate Change, (p. 1796),
731 Cambridge University Press. In Press, 2021.
732 Jayachandran, V., Nair, V., and Babu, S.: CCN characteristics over a tropical coastal station during
733 south-west monsoon: observations and closure studies, Atmos. Environ., 164, 299–308,
734 https://doi.org/10.1016/j.atmosenv.2017.06.012, 2017.
735 Jayachandran, V. N., Varghese, M., Murugavel, P., Todekar, K. S., Bankar, S. P., Malap, N., Dinesh,
736 G., Safai, P. D., Rao, J., Konwar, M., Dixit, S., and Prabha, T. V.: Cloud condensation nuclei
737 characteristics during the Indian summer monsoon over a rain-shadow region, Atmos. Chem.
738 Phys., 20, 7307–7334, https://doi.org/10.5194/acp-20-7307-2020, 2020.
739 Jia, H., Ma, X., Yu, F., Liu, Y., Yin, Y.: Distinct impacts of increased aerosols on cloud droplet
740 number concentration of stratus/stratocumulus and cumulus. Geophys. Res. Lett., 46(22):
741 13517–13525, https://doi.org/10.1029/2019GL085081, 2019.
742 Jurányi, Z., Tritscher, T., Gysel, M., Laborde, M., Gomes, L., Roberts, G., Baltensperger, U., and

https://doi.org/10.5194/acp-2022-427
Preprint. Discussion started: 27 June 2022

743 Weingartner, E.: Hygroscopic mixing state of urban aerosol derived from size-resolved cloud
744 condensation nuclei measurements during the MEGAPOLI campaign in Paris, Atmos. Chem.
745 Phys., 13, 6431–6446, https://doi.org/10.5194/acp-13-6431-2013, 2013.
746 Khain, P. A.: Notes on state-of-the-art investigations of aerosol effects on precipitation: A critical
747 review, Environ. Res. Lett., 4(1), 015004, DOI: 10.1088/1748-9326/4/1/015004, 2009.
748 Kim, J. H., Yum, S. S., Shim, S., Kim, W. J., Park, M., Kim, J.-H., Kim, M.-H., and Yoon, S.-C.: On
749 the submicron aerosol distributions and CCN number concentrations in and around the Korean
750 Peninsula, Atmos. Chem. Phys., 14, 8763–8779, https://doi.org/10.5194/acp-14-8763-2014,
751 2014.
752 Köhler, H.: The nucleus in and the growth of hygroscopic droplets, Trans Farad Soc, 32, 1152–1161,
753 https://doi.org/10.1039/TF9363201152, 1936.
754 Kristensen, T. B., Müller, T., Kandler, K., Benker, N., Hartmann, M., Prospero, J. M., Wiedensohler,
755 A., and Stratmann, F.: Properties of cloud condensation nuclei (CCN) in the trade wind marine
756 boundary layer of the western North Atlantic, Atmos. Chem. Phys., 16, 2675–2688,
757 https://doi.org/10.5194/acp-16-2675-2016, 2016.
758 Kuang, Y., He, Y., Xu, W., Zhao, P., Cheng, Y., Zhao, G., Tao, J., Ma, N., Su, H., Zhang, Y., Sun, J.,
759 Cheng, P., Yang, W., Zhang, S., Wu, C., Sun, Y., and Zhao, C.: Distinct diurnal variation in
760 organic aerosol hygroscopicity and its relationship with oxygenated organic aerosol, Atmos.
761 Chem. Phys., 20, 865–880, https://doi.org/10.5194/acp-20-865-2020, 2020.
762 Kulmala, M., Petäjä, T., Nieminen, T., Sipilä, M., Manninen, H. E., Lehtipalo, K., Dal Maso, M.,
763 Aalto, P. P., Junninen, H., Paasonen, P., Riipinen, I., Lehtinen, K. E. J., Laaksonen, A., and
764 Kerminen, V.-M.: Measurement of the nucleation of atmospheric aerosol particles, Nat.
765 Protocols, 7, 1651–1667, https://doi.org/10.1038/nprot.2012.091, 2012.
766 Liu, J. and Li, Z.: Estimation of cloud condensation nuclei concentration from aerosol optical
767 quantities: influential factors and uncertainties, Atmos. Chem. Phys., 14, 471–483,
768 https://doi.org/10.5194/acp-14-471-2014, 2014.
769 Lu, C., Niu, S., Liu, Y., and Vogelmann, A. M.: Empirical relationship between entrainment rate and
770 microphysics in cumulus clouds, Geophys. Res. Lett., 40(10), 2333-2338,
771 https://doi.org/10.1002/grl.50445, 2013.
772 Ma, N. and Birmili, W.: Estimating the contribution of photochemical particle formation to ultrafine
773 particle number averages in an urban atmosphere, Sci. Total Environ., 512/513, 154–166,
774 https://doi.org/10.1016/j.scitotenv.2015.01.009, 2015
775 Massling, A., Stock, M., Wehner, B., Wu, Z. J., Hu, M., Brueggemann, E., Gnauk, T., Herrmann, H.,
776 and Wiedensohler, A.: Size segregated water uptake of the urban submicrometer aerosol in
777 Beijing, Atmos. Environ., 43, 1578–1589, https://doi.org/10.1016/j.atmosenv.2008.06.003,
778 2009.
779 Mazoyer, M., Burnet, F., Denjean, C., Roberts, G. C., Haeffelin, M., Dupont, J.-C., and Elias, T.:
780 Experimental study of the aerosol impact on fog microphysics, Atmos. Chem. Phys., 19, 4323–

https://doi.org/10.5194/acp-2022-427
Preprint. Discussion started: 27 June 2022

4344, https://doi.org/10.5194/acp-19-4323-2019, 2019.

McFiggans, G., Artaxo, P., Baltensperger, U., Coe, H., Facchini, M. C., Feingold, G., Fuzzi, S., Gysel, M., Laaksonen, A., Lohmann, U., Mentel, T. F., Murphy, D. M., O'Dowd, C.D., Snider, J. R., and Weingartner, E.: The effect of physical and chemical aerosol properties on warm cloud droplet activation, Atmos. Chem. Phys., 6, 2593-2649, https://doi.org/10.5194/acp-6-2593-2006, 2006.

Müller, T., Henzing, J. S., de Leeuw, G., Wiedensohler, A., Alastuey, A., Angelov, H., Bizjak, M., Collaud Coen, M., Engström, J. E., Gruening, C., Hillamo, R., Hoffer, A., Imre, K., Ivanow, P., Jennings, G., Sun, J. Y., Kalivitis, N., Karlsson, H., Komppula, M., Laj, P., Li, S.-M., Lunder, C., Marinoni, A., Martins dos Santos, S., Moerman, M., Nowak, A., Ogren, J. A., Petzold, A., Pichon, J. M., Rodriquez, S., Sharma, S., Sheridan, P. J., Teinilä, K., Tuch, T., Viana, M., Virkkula, A., Weingartner, E., Wilhelm, R., and Wang, Y. Q.: Characterization and intercomparison of aerosol absorption photometers: result of two intercomparison workshops, Atmos. Meas. Tech., 4, 245–268, https://doi.org/10.5194/amt-4-245-2011, 2011

Nenes, A., Charlson, R. J., Facchini, M. C., Kulmalam M., Laaksonen, A., and Seinfeld, J. H.: Can chemical effects on cloud droplet number rival the first indirect effect? Geophys. Res. Lett., 29(17): 29-1-29-4, doi:10.1029/2002GL015295, 2002.

Ng, N. L., Herndon, S. C., Trimborn, A., Canagaratna, M. R., Croteau, P. L., Onasch, T. B., Sueper, D., Worsnop, D. R., Zhang, Q., Sun, Y. L., and Jayne, J. T.: An Aerosol Chemical Speciation Monitor (ACSM) for Routine Monitoring of the Composition and Mass Concentrations of Ambient Aerosol, Aerosol Sci. Tech., 45, 780–794, https://doi.org/10.1080/02786826.2011.560211, 2011.

Paramonov, M., Kerminen, V.-M., Gysel, M., Aalto, P. P., Andreae, M. O., Asmi, E., Baltensperger, U., Bougiatioti, A., Brus, D., Frank, G. P., Good, N., Gunthe, S. S., Hao, L., Irwin, M., Jaatinen, A., Jurányi, Z., King, S. M., Kortelainen, A., Kristensson, A., Lihavainen, H., Kulmala, M., Lohmann, U., Martin, S. T., McFiggans, G., Mihalopoulos, N., Nenes, A., O'Dowd, C. D., Ovadnevaite, J., Petäjä, T., Pöschl, U., Roberts, G. C., Rose, D., Svenningsson, B., Swietlicki, E., Weingartner, E., Whitehead, J., Wiedensohler, A., Wittbom, C., and Sierau, B.: A synthesis of cloud condensation nuclei counter (CCNC) measurements within the EUCAARI network, Atmos. Chem. Phys., 15, 12211–12229, https://doi.org/10.5194/acp-15-12211-2015, 2015.

Petters, M. D., and Kreidenweis, S. M.: A single parameter representation of hygroscopic growth and cloud condensation nuclei activity, Atmos. Chem. Phys., 7, 1961-1971, https://doi.org/10.5194/acp-7-1961-2007, 2007.

Petzold, A. and Schönlinner, M.: Multi-angle absorption photometry - a new method for the measurement of aerosol light absorption and atmospheric black carbon, J. Aerosol Sci., 35, 421–441, https://doi.org/10.1016/j.jaerosci.2003.09.005, 2004.

Poulain, L., Wu, Z., Petters, M. D., Wex, H., Hallbauer, E., Wehner, B., Massling, A., Kreidenweis, S. M., and Stratmann, F.: Towards closing the gap between hygroscopic growth and CCN

https://doi.org/10.5194/acp-2022-427
Preprint. Discussion started: 27 June 2022


Atmospheric Chemistry and Physics Discussions

activation for secondary organic aerosols – Part 3: Influence of the chemical composition on the hygroscopic properties and volatile fractions of aerosols, Atmos. Chem. Phys., 10, 3775–3785, https://doi.org/10.5194/acp-10-3775-2010, 2010.

Poulain, L., Spindler, G., Birmili, W., Plass-Dülmer, C., Wiedensohler, A., and Herrmann, H.: Seasonal and diurnal variations of particulate nitrate and organic matter at the IfT research station Melpitz, Atmos. Chem. Phys., 11, 12579–12599, https://doi.org/10.5194/acp-11-12579-2011, 2011.

Poulain, L., Spindler, G., Grüner, A., Tuch, T., Stieger, B., van Pinxteren, D., Petit, J.-E., Favez, O., Herrmann, H., and Wiedensohler, A.: Multi-year ACSM measurements at the central European research station Melpitz (Germany) – Part 1: Instrument robustness, quality assurance, and impact of upper size cutoff diameter, Atmos. Meas. Tech., 13, 4973–4994, https://doi.org/10.5194/amt-13-4973-2020, 2020.

Pöhlker, M. L., Pöhlker, C., Ditas, F., Klimach, T., Hrabe de Angelis, I., Araújo, A., Brito, J., Carbone, S., Cheng, Y., Chi, X., Ditz, R., Gunthe, S. S., Kesselmeier, J., Könemann, T., Lavrič, J. V., Martin, S. T., Mikhailov, E., Moran-Zuloaga, D., Rose, D., Saturno, J., Su, H., Thalman, R., Walter, D., Wang, J., Wolff, S., Barbosa, H. M. J., Artaxo, P., Andreae, M. O., and Pöschl, U.: Long-term observations of cloud condensation nuclei in the Amazon rain forest – Part 1: Aerosol size distribution, hygroscopicity, and new model parametrizations for CCN prediction, Atmos. Chem. Phys., 16, 15709–15740, https://doi.org/10.5194/acp-16-15709-2016, 2016.

Pöhlker, M. L., Ditas, F., Saturno, J., Klimach, T., Hrabě de Angelis, I., Araùjo, A. C., Brito, J., Carbone, S., Cheng, Y., Chi, X., Ditz, R., Gunthe, S. S., Holanda, B. A., Kandler, K., Kesselmeier, J., Könemann, T., Krüger, O. O., Lavrič, J. V., Martin, S. T., Mikhailov, E., Moran-Zuloaga, D., Rizzo, L. V., Rose, D., Su, H., Thalman, R., Walter, D., Wang, J., Wolff, S., Barbosa, H. M. J., Artaxo, P., Andreae, M. O., Pöschl, U., and Pöhlker, C.: Long-term observations of cloud condensation nuclei over the Amazon rain forest – Part 2: Variability and characteristics of biomass burning, long-range transport, and pristine rain forest aerosols, Atmos. Chem. Phys., 18, 10289–10331, https://doi.org/10.5194/acp-18-10289-2018, 2018.

Ramanathan, V., Crutzen, P. J., Kiehl, J. T., and Rosenfeld, D.: Aerosols, climate, and the hydrological cycle, Science, 294(5549), 2119–2124. https://doi.org/10.1126/science.1064034, 2001.

Rastak, N., Pajunoja, A., Acosta Navarro, J. C., Ma, J., Song, M., Partridge, D. G., Kirkevåg, A., Leong, Y., Hu, W. W., Taylor, N. F., Lambe, A., Cerully, K., Bougiatioti, A., Liu, P., Krejci, R., Petäjä, T., Percival, C., Davidovits, P., Worsnop, D. R., Ekman, A. M. L., Nenes, A., Martin, S., Jimenez, J. L., Collins, D. R., Topping, D. O., Bertram, A. K., Zuend, A., Virtanen, A., and Riipinen, I.: Microphysical explanation of the RH-dependent water affinity of biogenic organic aerosol and its importance for climate, Geophys. Res. Lett., 44, 5167–5177, https://doi.org/10.1002/2017gl073056, 2017.

Roberts, G. C., and Nenes, A.: A continuous-flow streamwise thermal-gradient CCN chamber for

https://doi.org/10.5194/acp-2022-427
Preprint. Discussion started: 27 June 2022

atmospheric measurements, Aerosol Sci. Tech., 39(3), 206–221, https://doi.org/10.1080/027868290913988, 2005.

Rose, D., Gunthe, S. S., Mikhailov, E., Frank, G. P., Dusek, U., Andreae, M. O., and Pöschl, U.: Calibration and measurement uncertainties of a continuous-flow cloud condensation nuclei counter (DMT-CCNC): CCN activation of ammonium sulfate and sodium chloride aerosol particles in theory and experiment, Atmos. Chem. Phys., 8, 1153–1179, https://doi.org/10.5194/acp-8-1153-2008, 2008.

Rose, D., Nowak, A., Achtert, P., Wiedensohler, A., Hu, M., Shao, M., Zhang, Y., Andreae, M. O., and Pöschl, U.: Cloud condensation nuclei in polluted air and biomass burning smoke near the mega-city Guangzhou, China – Part 1: Size-resolved measurements and implications for the modeling of aerosol particle hygroscopicity and CCN activity, Atmos. Chem. Phys., 10, 3365–3383, https://doi.org/10.5194/acp-10-3365-2010, 2010.

Rose, D., Gunthe, S. S., Su, H., Garland, R. M., Yang, H., Berghof, M., Cheng, Y. F., Wehner, B., Achtert, P., Nowak, A., Wiedensohler, A., Takegawa, N., Kondo, Y., Hu, M., Zhang, Y., Andreae, M. O., and Pöschl, U.: Cloud condensation nuclei in polluted air and biomass burning smoke near the megacity Guangzhou, China – Part 2: Size-resolved aerosol chemical composition, diurnal cycles, and externally mixed weakly CCN-active soot particles, Atmos. Chem. Phys., 11, 2817–2836, https://doi.org/10.5194/acp-11-2817-2011, 2011

Rosenfeld, D., Zhu, Y., Wang, M., Zheng, Y., Goren, T., and Yu, S.: Aerosol-driven droplet concentrations dominate coverage and water of oceanic low-level clouds, science, 363(6427), DOI: 10.1126/science.aav0566, 2019.

Salma, I., Thén, W., Vörösmarty, M., and Gyöngyösi, A. Z.: Cloud droplet activation in a continental Central European urban environment, Atmos. Chem. Phys. Discuss., https://doi.org/10.5194/acp-2021-305, in review, 2021.

Schmale, J., Henning, S., Decesari, S., Henzing, B., Keskinen, H., Sellegri, K., Ovadnevaite, J., Pöhlker, M. L., Brito, J., Bougiatioti, A., Kristensson, A., Kalivitis, N., Stavroulas, I., Carbone, S., Jefferson, A., Park, M., Schlag, P., Iwamoto, Y., Aalto, P., Äijälä, M., Bukowiecki, N., Ehn, M., Frank, G., Fröhlich, R., Frumau, A., Herrmann, E., Herrmann, H., Holzinger, R., Kos, G., Kulmala, M., Mihalopoulos, N., Nenes, A., O'Dowd, C., Petäjä, T., Picard, D., Pöhlker, C., Pöschl, U., Poulain, L., Prévôt, A. S. H., Swietlicki, E., Andreae, M. O., Artaxo, P., Wiedensohler, A., Ogren, J., Matsuki, A., Yum, S. S., Stratmann, F., Baltensperger, U., and Gysel, M.: Long-term cloud condensation nuclei number concentration, particle number size distribution and chemical composition measurements at regionally representative observatories, Atmos. Chem. Phys., 18, 2853–2881, https://doi.org/10.5194/acp-18-2853-2018, 2018.

Seinfeld, J. H., and Pandis, S. N.: Atmospheric chemistry and physics: From air pollution to climate change, Hoboken: John Wiley and Sons, 2016.

Sihto, S.-L., Mikkilä, J., Vanhanen, J., Ehn, M., Liao, L., Lehtipalo, K., Aalto, P. P., Duplissy, J., Petäjä, T., Kerminen, V.-M., Boy, M., and Kulmala, M.: Seasonal variation of CCN

https://doi.org/10.5194/acp-2022-427
Preprint. Discussion started: 27 June 2022

concentrations and aerosol activation properties in boreal forest, Atmos. Chem. Phys., 11, 13269–13285, https://doi.org/10.5194/acp-11-13269-2011, 2011.

Singla, V., Mukherjee, S., Safai, P. D., Meena, G. S., Dani, K. K., Pandithurai, G.: Role of organic aerosols in CCN activation and closure over a rural background site in Western Ghats, India, Atmos. Environ., 158, 148-159, https://doi.org/10.1016/j.atmosenv.2017.03.037, 2017.

Stokes, R. H. and Robinson, R. A.: Interactions in Aqueous Nonelectrolyte Solutions. I. Solute-Solvent Equilibria, J. Phys. Chem., 70, 2126–2130, DOI: 10.1021/j100879a010, 1966.

Su, H., Rose, D., Cheng, Y. F., Gunthe, S. S., Massling, A., Stock, M., Wiedensohler, A., Andreae, M. O., and Pöschl, U.: Hygroscopicity distribution concept for measurement data analysis and modeling of aerosol particle mixing state with regard to hygroscopic growth and CCN activation, Atmos. Chem. Phys., 10, 7489–7503, https://doi.org/10.5194/acp-10-7489-2010, 2010.

Twomey, S.: The nuclei of natural cloud formation part II: The supersaturation in natural clouds and the variation of cloud droplet concentration, Geofisica Pura e Applicata, 43, 243–249, DOI: 10.1007/BF01993560, 1959.

Twomey, S.: Pollution and the planetary albedo, Atmos. Environ., 8(12), 1251–1256, https://doi.org/10.1016/0004-6981(74)90004-3, 1974.

Twomey, S.: The influence of pollution on the shortwave albedo of clouds, J. Atmos. Sci., 34(7), 1149–1152, https://doi.org/10.1175/1520-0469(1977)034<1149:TIOPOT>2.0.CO;2, 1977.

Tuch, T. M., Haudek, A., Müller, T., Nowak, A., Wex, H., and Wiedensohler, A.: Design and performance of an automatic regenerating adsorption aerosol dryer for continuous operation at monitoring sites, Atmos. Meas. Tech., 2, 417–422, https://doi.org/10.5194/amt-2-417-2009, 2009.

Varghese, M., Prabha, T. V., Malap, N., Resmi, E. A., Murugavel, P., Safai, P. D., Axisa, D., Pandithurai, G., and Dani, K.: Airborne and ground based CCN spectral characteristics: Inferences from CAIPEEX–2011, Atmos. Environ., 125, 324–336, https://doi.org/10.1016/j.atmosenv.2015.06.041, 2016

Wang, Y., Wan, Q., Meng, W., Liao, F., Tan, H., and Zhang, R.: Long-term impacts of aerosols on precipitation and lightning over the Pearl River Delta megacity area in China, Atmos. Chem. Phys., 11, 12421–12436, https://doi.org/10.5194/acp-11-12421-2011, 2011.

Wang, Y., Wang, M., Zhang, R., Ghan, S. J., Lin, Y., Hu, J., Pan, B., Levy, M., Jiang, J. H., and Molina, M. J.: Assessing the effects of anthropogenic aerosols on Pacific storm track using a multiscale global climate model, Proc. Natl. Acad. Sci. U.S.A., 111(19), 6894–6899, https://doi.org/10.1073/pnas.1403364111, 2014.

Wang, Y., Li, Z., Zhang, Y., Du, W., Zhang, F., Tan, H., Xu, H., Fan, T., Jin, X., Fan, X., Dong, Z., Wang, Q., and Sun, Y.: Characterization of aerosol hygroscopicity, mixing state, and CCN activity at a suburban site in the central North China Plain, Atmos. Chem. Phys., 18, 11739–11752, https://doi.org/10.5194/acp-18-11739-2018, 2018a.

https://doi.org/10.5194/acp-2022-427
Preprint. Discussion started: 27 June 2022


Atmospheric Chemistry and Physics Discussions

933 Wang, Y., Wu, Z., Ma, N., Wu, Y., Zeng, L., Zhao, C., and Wiedensohler, A.: Statistical analysis and
934 parameterization of the hygroscopic growth of the sub-micrometer urban background aerosol
935 in Beijing, Atmos. Environ., 175, 184–191, https://doi.org/10.1016/j.atmosenv.2017.12.003,
936 2018b.
937 Wang, Y., Niu, S., Lv, J., Lu, C., Xu, X., Wang, Y., Ding, J., Zhang, H., Wang, T., and Kang, B.: A
938 new method for distinguishing unactivated particles in cloud condensation nuclei
939 measurements: Implications for aerosol indirect effect evaluation, Geophys. Res. Lett., 46,
940 14,185–14,194, https://doi.org/10.1029/2019GL085379, 2019.
941 Wang, Z., Birmili, W., Hamed, A., Wehner, B., Spindler, G., Pei, X., Wu, Z., Cheng, Y., Su, H., and
942 Wiedensohler, A.: Contributions of volatile and nonvolatile compounds (at 300°C) to
943 condensational growth of atmospheric nanoparticles: An assessment based on 8.5 years of
944 observations at the Central Europe background site Melpitz, J. Geophys. Res. Atmos., 122,
945 485–497, doi:10.1002/2016JD025581, 2017.
946 Wiedensohler, A.: An approximation of the bipolar charge distribution for particles in the sub-
947 micron size range, J. Aerosol Sci., 19, 387–389, DOI: 10.1016/0021-8502(88)90278-9, 1988.
948 Wiedensohler, A., Birmili, W., Nowak, A., Sonntag, A., Weinhold, K., Merkel, M., Wehner, B., Tuch,
949 T., Pfeifer, S., Fiebig, M., Fjäraa, A. M., Asmi, E., Sellegri, K., Depuy, R., Venzac, H., Villani,
950 P., Laj, P., Aalto, P., Ogren, J. A., Swietlicki, E., Williams, P., Roldin, P., Quincey, P., Hüglin,
951 C., Fierz-Schmidhauser, R., Gysel, M., Weingartner, E., Riccobono, F., Santos, S., Grüning, C.,
952 Faloon, K., Beddows, D., Harrison, R., Monahan, C., Jennings, S. G., O'Dowd, C. D., Marinoni,
953 A., Horn, H.-G., Keck, L., Jiang, J., Scheckman, J., McMurry, P. H., Deng, Z., Zhao, C. S.,
954 Moerman, M., Henzing, B., de Leeuw, G., Löschau, G., and Bastian, S.: Mobility particle size
955 spectrometers: harmonization of technical standards and data structure to facilitate high quality
956 long-term observations of atmospheric particle number size distributions, Atmos. Meas. Tech.,
957 5, 657–685, https://doi.org/10.5194/amt-5-657-2012, 2012.
958 Wiedensohler, A., Wiesner, A., Weinhold, K., Birmili, W., Hermann, M., Merkel, M., Muller, T.,
959 Pfeifer, S., Schmidt, A., Tuch, T., Velarde, F., Quincey, P., Seeger, S., and Nowak, A.: Mobility
960 particle size spectrometers: Calibration procedures and measurement uncertainties, Aerosol Sci.
961 Tech., 52, 146–164, https://doi.org/10.1080/02786826.2017.1387229, 2018.
962 Wu, Z. J., Poulain, L., Birmili, W., Größ, J., Niedermeier, N., Wang, Z. B., Herrmann, H., and
963 Wiedensohler, A.: Some insights into the condensing vapors driving new particle growth to
964 CCN sizes on the basis of hygroscopicity measurements, Atmos. Chem. Phys., 15, 13071–
965 13083, https://doi.org/10.5194/acp-15-13071-2015, 2015.
966 Wu, Z. J., Zheng, J., Shang, D. J., Du, Z. F., Wu, Y. S., Zeng, L. M., Wiedensohler, A., and Hu, M.:
967 Particle hygroscopicity and its link to chemical composition in the urban atmosphere of Beijing,
968 China, during summertime, Atmos. Chem. Phys., 16, 1123–1138, https://doi.org/10.5194/acp-
969 16-1123-2016, 2016.
970 Ye, X., Tang, C., Yin, Z., Chen, J., Ma, Z., Kong, L., Yang, X., Gao, W., and Geng, F.: Hygroscopic

https://doi.org/10.5194/acp-2022-427
Preprint. Discussion started: 27 June 2022

growth of urban aerosol particles during the 2009 Mirage-Shanghai Campaign, Atmos. Environ., 64, 263–269, https://doi.org/10.1016/j.atmosenv.2012.09.064, 2013.

Zdanovskii, B.: Novyi Metod Rascheta Rastvorimostei Elektrolitovv Mnogokomponentnykh Sistema, Zh. Fiz. Khim+, 22, 1478–1485, 1486–1495, 1948.

Zhang, F., Li, Y., Li, Z., Sun, L., Li, R., Zhao, C., Wang, P., Sun, Y., Liu, X., Li, J., Li, P., Ren, G., and Fan, T.: Aerosol hygroscopicity and cloud condensation nuclei activity during the AC3Exp campaign: implications for cloud condensation nuclei parameterization, Atmos. Chem. Phys., 14, 13423–13437, https://doi.org/10.5194/acp-14-13423-2014, 2014.

Zhang, F., Li, Z., Li, Y., Sun, Y., Wang, Z., Li, P., Sun, L., Wang, P., Cribb, M., Zhao, C., Fan, T., Yang, X., and Wang, Q.: Impacts of organic aerosols and its oxidation level on CCN activity from measurement at a suburban site in China, Atmos. Chem. Phys., 16, 5413–5425, https://doi.org/10.5194/acp-16-5413-2016, 2016.

Zhang, F., Wang, Y., Peng, J., Ren, J., Collins, D., Zhang, R., Sun, Y., Yang, X., and Li, Z.: Uncertainty in predicting CCN activity of aged and primary aerosols, J. Geophys. Res. Atmos., 122(21): 11,723-11,736, https://doi.org/10.1002/2017JD027058, 2017.

Zhao, C., Klein, S. A., Xie, S., Liu, X., Boyle, J. S., and Zhang, Y.: Aerosol first indirect effects on non-precipitating low-level liquid cloud properties as simulated by CAM5 at ARM sites, Geophys. Res. Lett., 39, L08806, https://doi.org/10.1029/2012GL051213, 2012.

Zhao, C., and Garrett, T. J.: Effects of Arctic haze on surface cloud radiative forcing, Geophys. Res. Lett., 42(2), 557–564, https://dx.doi.org/10.1002/2014GL062015, 2015

https://doi.org/10.5194/acp-2022-427
Preprint. Discussion started: 27 June 2022

Atmospheric Chemistry and Physics Discussions

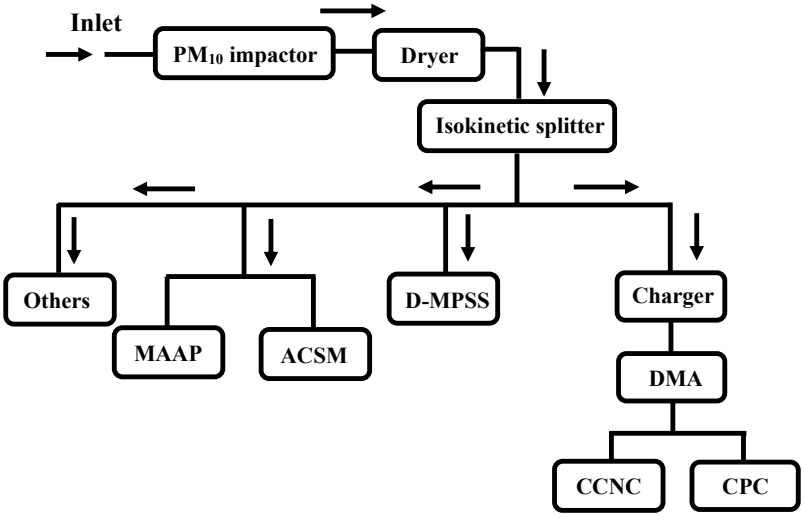

992

993 Figure 1. Schematic diagram of the experimental setup. D-MPSS — Dual-mobility particle size
994 spectrometer, ACSM — aerosol chemical species monitor, MAAP — multi-angle absorption
995 photometer, DMA — differential mobility analyzer, CPC — condensation particle counter, CCNC
996 — cloud condensation nuclei counter.

997

https://doi.org/10.5194/acp-2022-427
Preprint. Discussion started: 27 June 2022

Atmospheric Chemistry and Physics Discussions

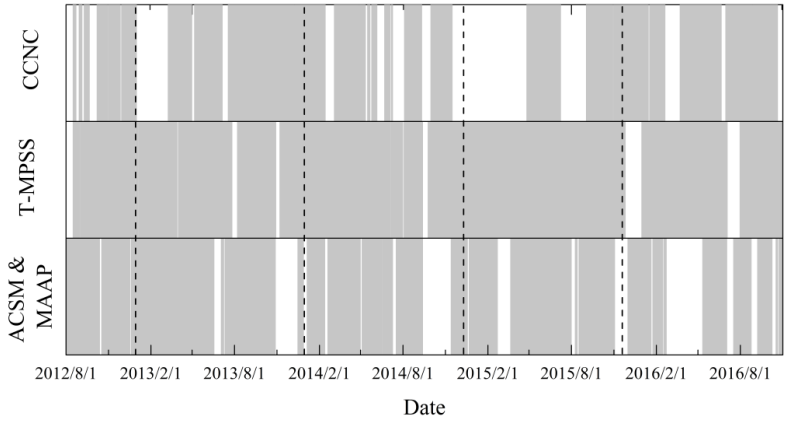

998

999 Figure 2. Coverage of the effective data represented by the gray columns.

1000

https://doi.org/10.5194/acp-2022-427
Preprint. Discussion started: 27 June 2022

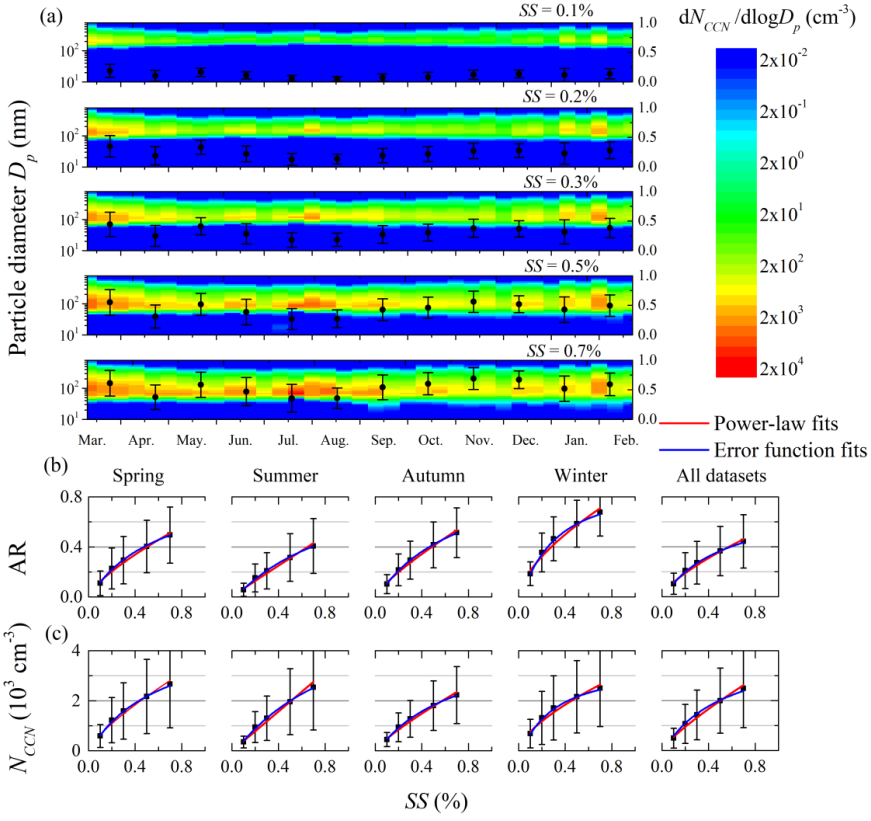

Figure 3. Seasonal variations of (a) CCN number size distributions and activation ratios (AR) at five different supersaturation (*SS*) conditions, (b) relationship between AR and *SS* for different seasons, and (c) relationship between CCN number concentration (N_{CCN}) and *SS* for different seasons. Error bar means one standard deviation. Red lines and blue lines are the fittings for AR vs. *SS* and N_{CCN} vs. *SS* with using the power-law function and the error function, respectively. Fitting results are shown in Table 3.

https://doi.org/10.5194/acp-2022-427
Preprint. Discussion started: 27 June 2022

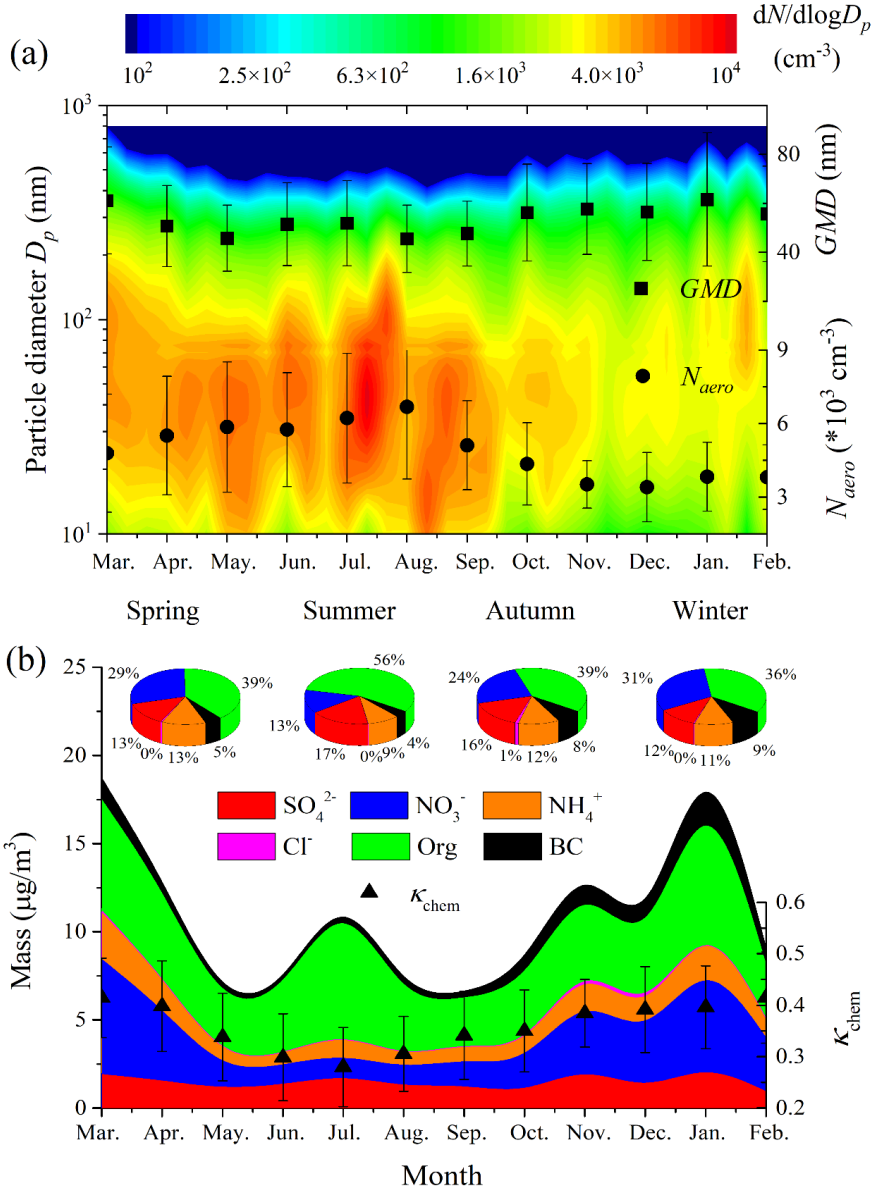

Figure 4. Seasonal variations of (a) aerosol physical and (b) chemical properties. dN_{aero}/dlog$D$ represents the aerosol number concentration at each bin, *GMD* is the geometric mean diameter of the particles, N_{aero} means total aerosol number concentration with diameter ranging 10 to 800 nm, κ_{chem} is the hygroscopicity factor calculated from the chemical composition. Error bar is one standard derivation.

https://doi.org/10.5194/acp-2022-427
Preprint. Discussion started: 27 June 2022

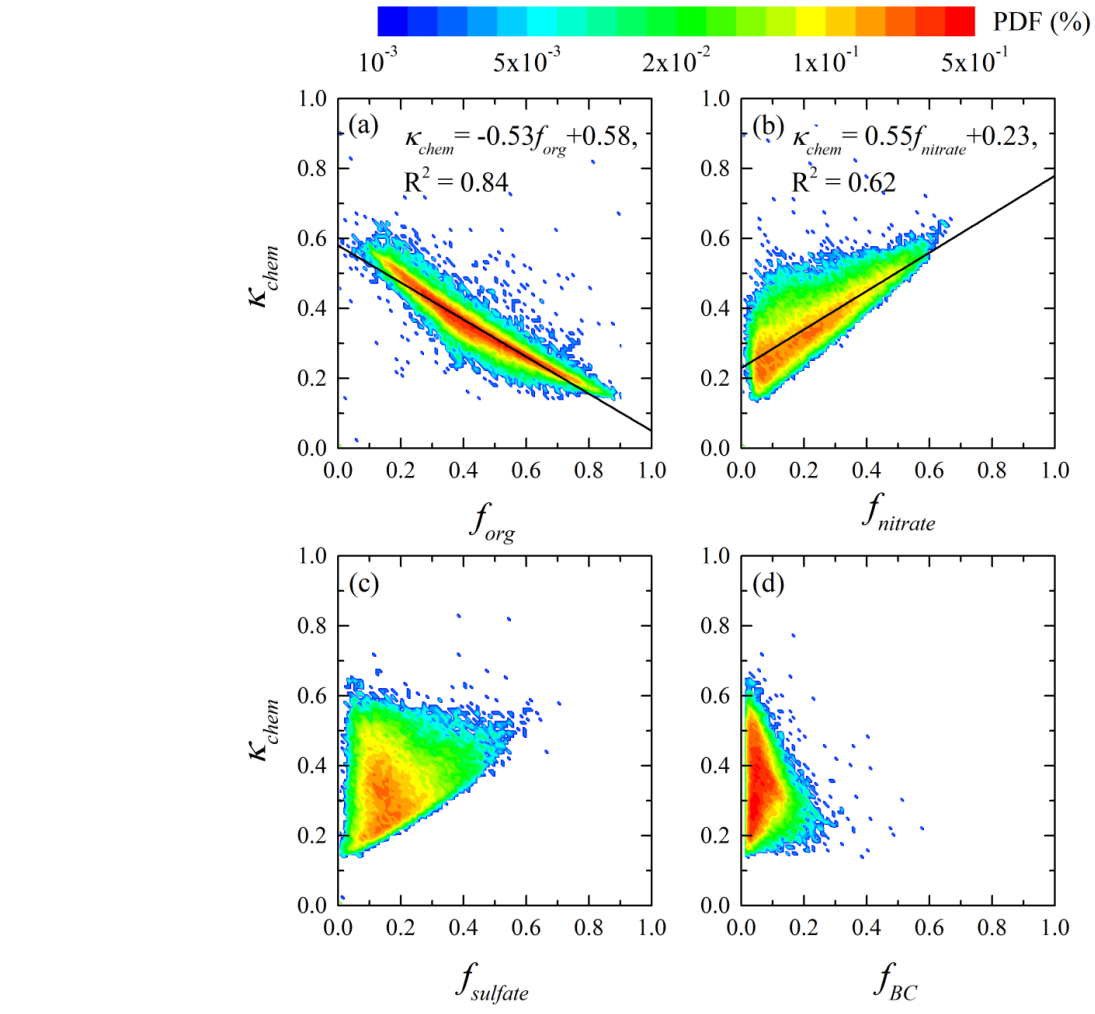

Figure 5. Relationships between (a) aerosol hygroscopicity factor calculated from the chemical composition (κ_{chem}) and mass fraction of organics (f_{org}) in submicron aerosol, (b) κ_{chem} vs. mass fraction of nitrate ($f_{nitrate}$), (c) κ_{chem} vs. mass fraction of nitrate ($f_{sulfate}$), and (d) κ_{chem} vs. mass fraction of black carbon (f_{BC}). Color bar represents the probability density function (PDF). Black lines are linear fit lines.

https://doi.org/10.5194/acp-2022-427
Preprint. Discussion started: 27 June 2022

Atmospheric Chemistry and Physics Discussions

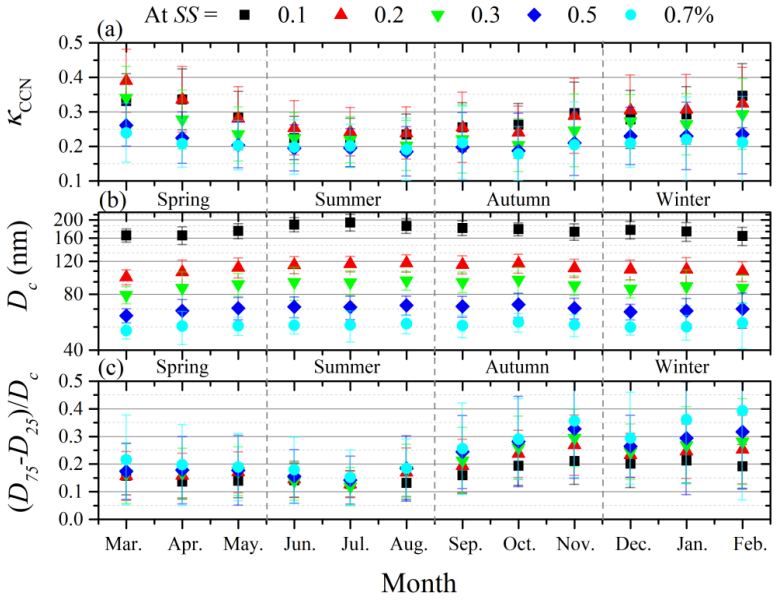

Figure 6. Monthly average of (a) hygroscopicity factor calculated from monodisperse CCN measurements (κ_{CCN}), (b) critical diameter of dry particle for activation (D_c), and (c) the degree of external mixture ($(D_{75} - D_{25})/D_c$) at five different supersaturation (SS) conditions. The definitions of D_{75} and D_{25} are the D_p at which 75% and 25% of the particles are activated at the given SS, respectively. Error bar is one standard derivation.

https://doi.org/10.5194/acp-2022-427
Preprint. Discussion started: 27 June 2022

Atmospheric Chemistry and Physics Discussions

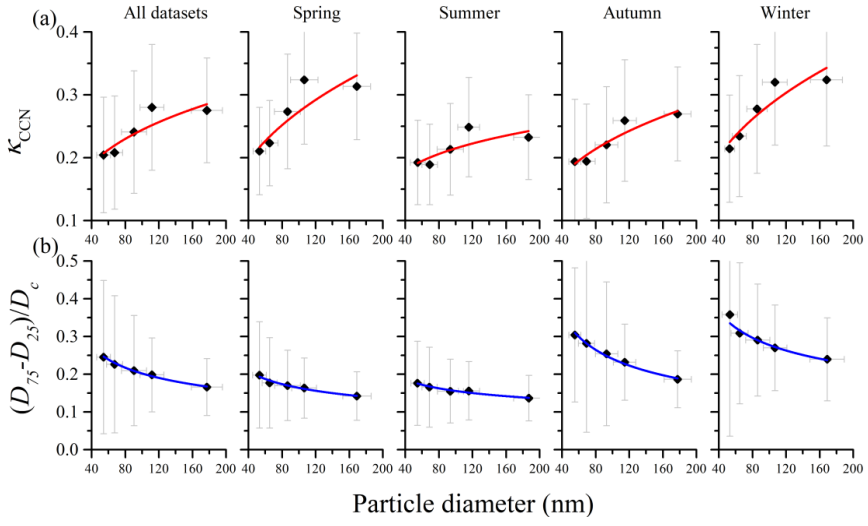

Figure 7. (a) Relationship between the particle diameter (D_p) and hygroscopicity factor calculated from monodisperse CCN measurements (κ_{CCN}), and (b) D_p vs. degree of external mixture (($D_{75} - D_{25}$)/D_c) at each season. The definitions of D_{75} and D_{25} are the D_p at which 75% and 25% of the particles are activated at the given *SS*, respectively. Red and blue lines are power-law fits for κ_{CCN} vs. D_p and $(D_{75} - D_{25})/D_c$ vs. D_p.

https://doi.org/10.5194/acp-2022-427
Preprint. Discussion started: 27 June 2022

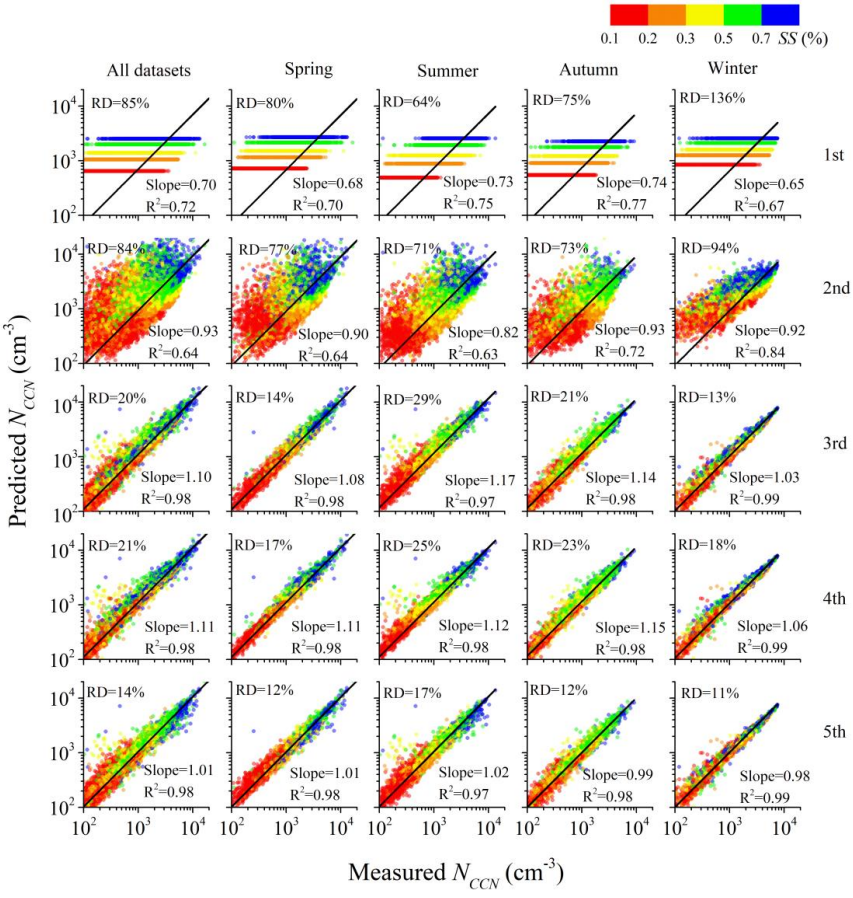

Figure 8. Predicted vs. measured CCN number concentration (N_{CCN}) for different seasons. The Predicted N_{CCN} is calculated from five different schemes with a detailed introduction shown in Table 6. Color bar represents the different supersaturation (*SS*) conditions. Black lines are the linear fits. The slope and R^2 of the linear regression and the relative deviation (RD) of the predicted N_{CCN} (RD= (|predicted N_{CCN} – measured N_{CCN}|)/measured N_{CCN}) are shown in each panel. Each row represents the results at the same scheme in different seasons; each column represents the results at different schemes in the same season.

https://doi.org/10.5194/acp-2022-427
Preprint. Discussion started: 27 June 2022

Atmospheric Chemistry and Physics Discussions

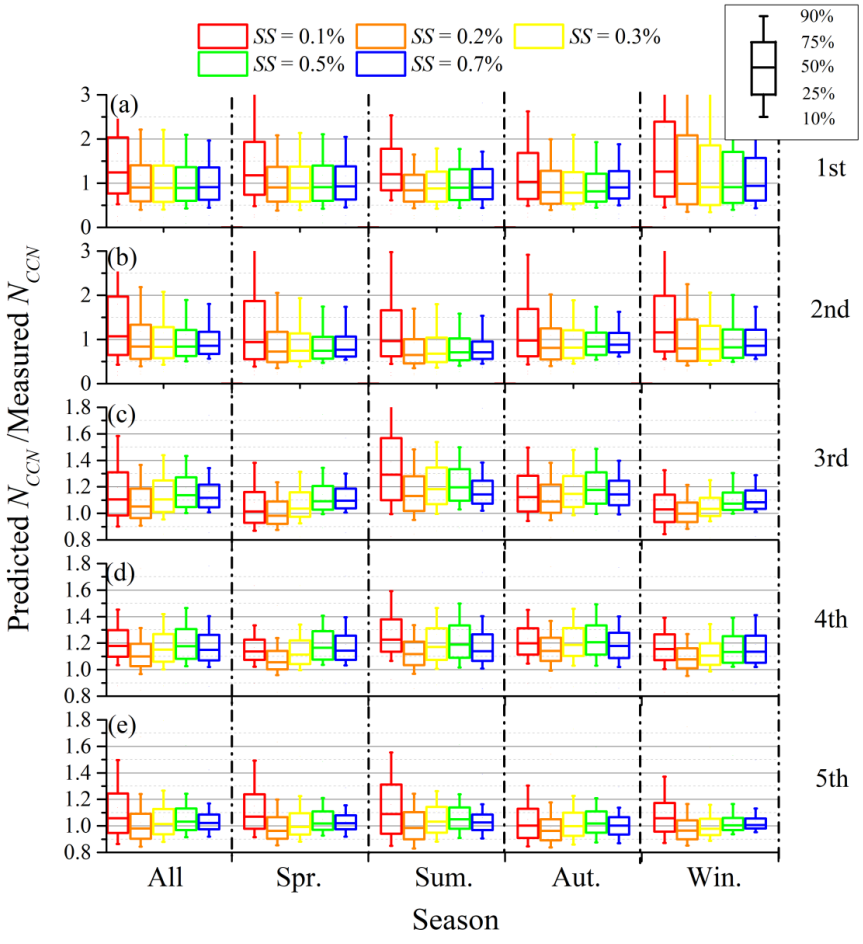

Figure 9. Statistics of the ratio of predicted CCN number concentration (N_{CCN}) to the measured one at different supersaturation (*SS*) conditions for each season and all datasets. The (a), (b), (c), (d), and (e) represent the prediction results from the 1st, 2nd, 3rd, 4th, and 5th scheme, respectively.

https://doi.org/10.5194/acp-2022-427
Preprint. Discussion started: 27 June 2022

Atmospheric Chemistry and Physics Discussions

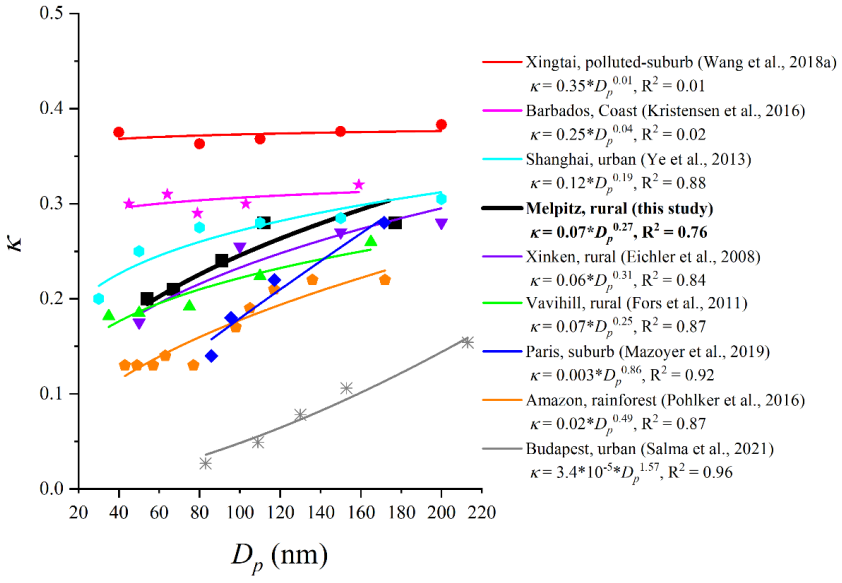

Figure 10. Relationships between the particle hygroscopicity factor (κ) and diameter (D_p) observed at different aerosol background regions. Lines are the power-law fits of κ vs. D_p.

https://doi.org/10.5194/acp-2022-427
Preprint. Discussion started: 27 June 2022

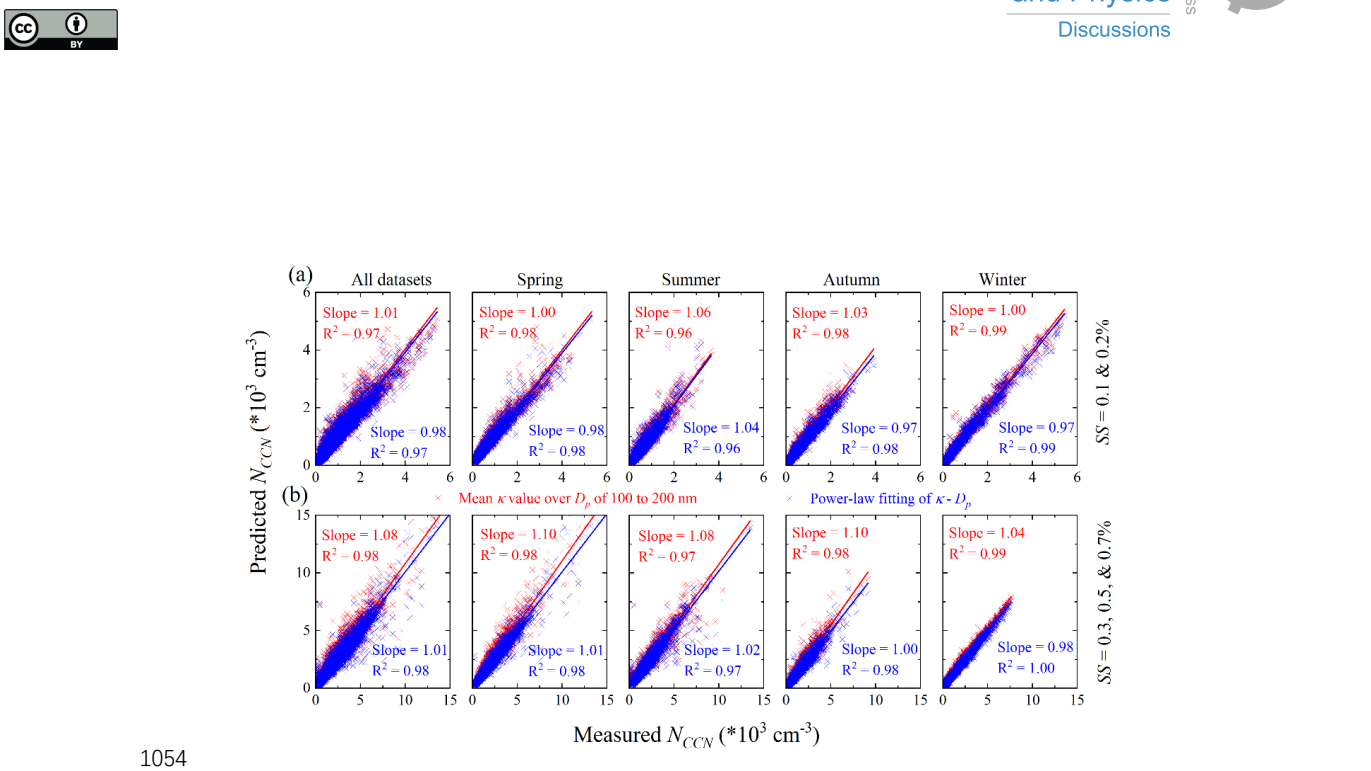

Figure 11. Predicted vs. measured CCN number concentration (N_{CCN}) at different supersaturation (SS) conditions for different seasons. (a) represents the results at SS = 0.1 and 0.2%; (b) shows the results at SS = 0.3, 0.5, and 0.7%. Red cross represents the predicted N_{CCN} using mean hygroscopicity factor (κ) over particle diameter (D_p) of 100 to 200 nm, while the blue cross represents the predicted N_{CCN} using power-law fit of κ and D_p. Red and blue lines are the linear fits.

https://doi.org/10.5194/acp-2022-427
Preprint. Discussion started: 27 June 2022

Atmospheric Chemistry and Physics Discussions

1061 Table 1. Densities (ρ) and hygroscopicity factor (κ) for each component.

Species	NH_4NO_3	$(NH_4)_2SO_4$	NH_4HSO_4	H_2SO_4	Organics	BC
ρ (kg m^{-3})	1720	1769	1780	1830	1400	1700
κ	0.67	0.61	0.61	0.92	0.1	0

1062

https://doi.org/10.5194/acp-2022-427
Preprint. Discussion started: 27 June 2022

1063 Table 2. Summary of CCN number concentration (N_{CCN}) at different supersaturation (SS) conditions
1064 measured at different locations.

Location (coordinates; a.m.s.l)	Type	Period	SS (%)	Mean N_{CCN} (cm^{-3})	Reference
Melpitz, Germany (51.5°N, 12.9°E; 86 m)	rural, continental	Aug. 2012–Oct. 2016	0.1 0.2 0.3 0.5 0.7	513 1102 1466 2020 2477	Present study
Vavihill, Sweden (56.0°N, 13.2 °E; 172 m)	rural	May 2008–Jul 2010	0.1–1.0	362–1795	Fors et al., 2011
Southern Great Plains, USA (36.6°N, 97.5°W; 320 m)	rural, agricultural	Sep. 2006–Apr. 2011	0.4	1248	Liu and Li, 2014
Hyytiälä, Finland (61.9°N, 24.3°E; 181 m)	rural	Feb. 2009–Dec. 2012	0.1–1.0	274–1128	Paramonov et al., 2015
Mahabaleshwar, India (17.9°N, 73.7°E; ~490 m)	rural	Jun. 2015	0.1–0.94	118–1826	Singla et al., 2017
Guangzhou, China (23.6°N, 113.1°E; ~21 m)	rural	Jul. 2006	0.068–0.67	995–10731	Rose et al., 2010
Wuqing, China (39.4°N, 117.0°E; 7.4 m)	suburban	Dec. 2009–Jan. 2010	0.056–0.7	2192–12963	Deng et al., 2011
Seoul, Korea (37.6°N, 127.0°E; ~38 m)	urban	2004–2010	0.4–0.8	4145–6067	Kim et al., 2014
Mahabubnagar, India (17.7°N, 78.9°E; ~490 m)	polluted continental	Oct. 2011	1.0	~5400	Varghese et al., 2016

1065

https://doi.org/10.5194/acp-2022-427
Preprint. Discussion started: 27 June 2022

Atmospheric Chemistry and Physics Discussions

Table 3. Power-law function fits and error function fits for the relationships between activation ratio (AR) vs. supersaturation (*SS*), and CCN number concentration (N_{CCN}) vs. *SS* for different seasons.

Season	*AR* vs. *SS*		N_{CCN} vs. *SS*	
	Power-law	*Error Function*	*Power-law*	*Error Function*
Spring	$AR=0.66SS^{0.73}$, $R^2=0.98$	$AR=0.5+0.50\mathrm{erf}(\ln(SS/0.72)/2.33)$, $R^2=0.998$	$N_{CCN}=3679SS^{0.76}$, $R^2=0.97$	$N_{CCN}=2637+2637\mathrm{erf}(\ln(SS/0.72)/2.33)$, $R^2=0.998$
Summer	$AR=0.61SS^{0.97}$, $R^2=0.97$	$AR=0.51+0.51\mathrm{erf}(\ln(SS/1.04)/2.15)$, $R^2=0.997$	$N_{CCN}=3951SS^{1.01}$, $R^2=0.96$	$N_{CCN}=3162+3162\mathrm{erf}(\ln(SS/1.04)/2.15)$, $R^2=0.997$
Autumn	$AR=0.71SS^{0.79}$, $R^2=0.98$	$AR=0.56+0.56\mathrm{erf}(\ln(SS/0.84)/2.29)$, $R^2=0.999$	$N_{CCN}=3136SS^{0.81}$, $R^2=0.98$	$N_{CCN}=2433+24336\mathrm{erf}(\ln(SS/0.84)/2.29)$, $R^2=0.999$
Winter	$AR=0.89SS^{0.63}$, $R^2=0.96$	$AR=0.44+0.44\mathrm{erf}(\ln(SS/0.29)/1.83)$, $R^2=0.999$	$N_{CCN}=3325SS^{0.64}$, $R^2=0.96$	$N_{CCN}=1624+1624\mathrm{erf}(\ln(SS/0.29)/1.83)$, $R^2=0.999$
All	$AR=0.59SS^{0.71}$, $R^2=0.98$	$AR=0.40+0.40\mathrm{erf}(\ln(SS/0.59)/2.25)$, $R^2=0.998$	$N_{CCN}=3497SS^{0.81}$, $R^2=0.98$	$N_{CCN}=2199+2199\mathrm{erf}(\ln(SS/0.59)/2.25)$, $R^2=0.998$

https://doi.org/10.5194/acp-2022-427
Preprint. Discussion started: 27 June 2022

Atmospheric Chemistry and Physics Discussions

Table 4. At each supersaturation (*SS*) condition, seasonal mean values of the hygroscopicity factor calculated from monodisperse CCN measurements (κ_{CCN}), the critical diameter of dry particle for activation (D_c), and the degree of external mixture ($(D_{75} - D_{25})/D_c$). The unit of D_c is nm.

Parameters	*SS* (%)	All datasets	Spring	Summer	Autumn	Winter
κ_{CCN}	0.1	0.28	0.31	0.23	0.27	0.32
	0.2	0.28	0.32	0.25	0.26	0.32
	0.3	0.24	0.27	0.21	0.22	0.28
	0.5	0.21	0.22	0.19	0.19	0.23
	0.7	0.20	0.21	0.19	0.19	0.21
D_c	0.1	177	169	187	178	168
	0.2	112	107	116	115	107
	0.3	91	87	94	93	86
	0.5	67	65	69	69	64
	0.7	54	53	55	55	53
$(D_{75} - D_{25})/D_c$	0.1	0.17	0.14	0.14	0.19	0.24
	0.2	0.20	0.16	0.16	0.23	0.27
	0.3	0.21	0.17	0.15	0.25	0.29
	0.5	0.23	0.18	0.17	0.28	0.31
	0.7	0.25	0.20	0.18	0.30	0.36

https://doi.org/10.5194/acp-2022-427
Preprint. Discussion started: 27 June 2022

Atmospheric Chemistry and Physics Discussions

1073 Table 5. Power-law fit results in Figure 7. The unit of particle diameter (D_p) is nm.

	κ_{CCN} vs. D_p	$(D_{75} - D_{25})/D_c$ vs. D_p
All datasets	$y = 0.07\ x^{0.27}$, $R^2 = 0.76$	$y = 0.92\ x^{-0.33}$, $R^2 = 0.99$
Spring	$y = 0.05\ x^{0.37}$, $R^2 = 0.76$	$y = 0.55\ x^{-0.26}$, $R^2 = 0.97$
Summer	$y = 0.09\ x^{0.19}$, $R^2 = 0.56$	$y = 0.39\ x^{-0.20}$, $R^2 = 0.95$
Autumn	$y = 0.05\ x^{0.31}$, $R^2 = 0.88$	$y = 1.70\ x^{-0.42}$, $R^2 = 0.99$
Winter	$y = 0.05\ x^{0.36}$, $R^2 = 0.82$	$y = 1.10\ x^{-0.30}$, $R^2 = 0.95$

1074

https://doi.org/10.5194/acp-2022-427
Preprint. Discussion started: 27 June 2022

Atmospheric Chemistry and Physics Discussions

1075 Table 6. Introduction of five activation schemes. The meaning of the abbreviation can be found in
1076 Notation list.

Category	Scheme	Introduction
1st category: N_{CCN} - SS or AR - SS empirical fit	1st	N_{CCN} - SS power-law fits shown in Table 3
	2nd	Real-time N_{aero} combined with AR - SS power-law fits shown in Table 3
2nd category: Real-time PNSD combined with the parameterized κ	3rd	Real-time PNSD combined with a constant κ of 0.3
	4th	Real-time PNSD combined with the real-time bulk κ_{chem}
	5th	Real-time PNSD combined with κ - D_p power-law fits shown in Table 5

1077

1078

https://doi.org/10.5194/acp-2022-427
Preprint. Discussion started: 27 June 2022

Atmospheric Chemistry and Physics Discussions

1079 **Appendix A**

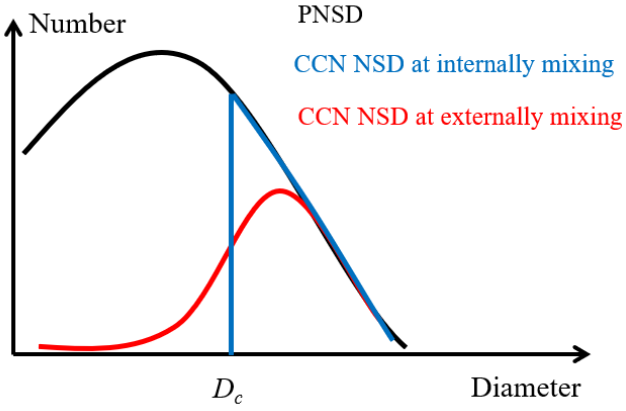

1080

1081 Figure A1. Schematic diagram for the relationship among the particle number size distribution
1082 (PNSD), CCN number size distribution (CCN NSD) at internally mixing, and the CCN NSD at
1083 externally mixing.

1084